PIXWIZARD: VERSATILE IMAGE-TO-IMAGE VISUAL ASSISTANT WITH OPEN-LANGUAGE INSTRUCTIONS

Anonymous authors
Paper under double-blind review

ABSTRACT

This paper presents a versatile image-to-image visual assistant, **PixWizard**, designed for image generation, manipulation, and translation based on free-from language instructions. To this end, we tackle a variety of vision tasks into a unified image-text-to-image generation framework and curate an *Omni Pixel-to-Pixel Instruction-Tuning Dataset*. By constructing detailed instruction templates in natural language, we comprehensively include a large set of diverse vision tasks such as text-to-image generation, image restoration, image grounding, dense image prediction, image editing, controllable generation, inpainting/outpainting, and more. Furthermore, we adopt Diffusion Transformers (DiT) as our foundation model and extend its capabilities with a flexible any resolution mechanism, enabling the model to dynamically process images based on the aspect ratio of the input, closely aligning with human perceptual processes. The model also incorporates structure-aware and semantic-aware guidance to facilitate effective fusion of information from the input image. Our experiments demonstrate that PixWizard not only shows impressive generative and understanding abilities for images with diverse resolutions but also exhibits promising generalization capabilities with unseen tasks and human instructions.

1 INTRODUCTION

Large Language Models (LLMs) (Brown et al., 2020; Touvron et al., 2023) and Large Vision Models (LVMs) (Radford et al., 2021; Caron et al., 2021; Bai et al., 2024) have gained global popularity by successfully unifying multiple tasks within a single, coherent framework. Nowadays, LLMs have become efficient language assistants, demonstrating strong capabilities in open-world language understanding and reasoning. However, a versatile visual assistant capable of following diverse multimodal instructions that align with human intentions to effectively perform various visual tasks in real-world scenarios is still under exploration.

Recently, there are two research lines aiming to achieve general visual assistants: diffusion-based and in-context learning approaches. The first focuses on developing text-to-image models (Rombach et al., 2022b) as a unified foundation model for various visual perception tasks. For example, InstructPix2Pix (Brooks et al., 2023), InstructDiffusion (Geng et al., 2024), and InstructCV (Gan et al., 2024) repurpose generative models as a universal language interface for image editing and other visual tasks. However, their capable tasks are limited, and their performance lags behind that of task-specific models. The second research direction focuses on visual prompting, where pixel-based prompts are used to tackle various vision tasks within a single learning framework. This approach employs prompting techniques to generate the desired visual outputs in an in-context manner. Examples include Painter (Wang et al., 2023b), PromptDiffusion (Wang et al., 2023c), and LVM (Bai et al., 2024), which have successfully handled a variety of visual scenarios within one framework. However, these methods inherently lack the ability to follow human language instructions, limiting their controllability and interactivity. (More related works are discussed in Sec. A.)

Taking into account the strengths and limitations of previous approaches, we introduce **PixWizard**, a versatile interactive image-to-image visual assistant designed for image generation, manipulation, and image-to-image translation. PixWizard is a DiT-based framework that can handle a wide range of visual tasks when provided with sufficient training data, along with the interface for human language instructions. Specifically, PixWizard exhibits three main features as follows:

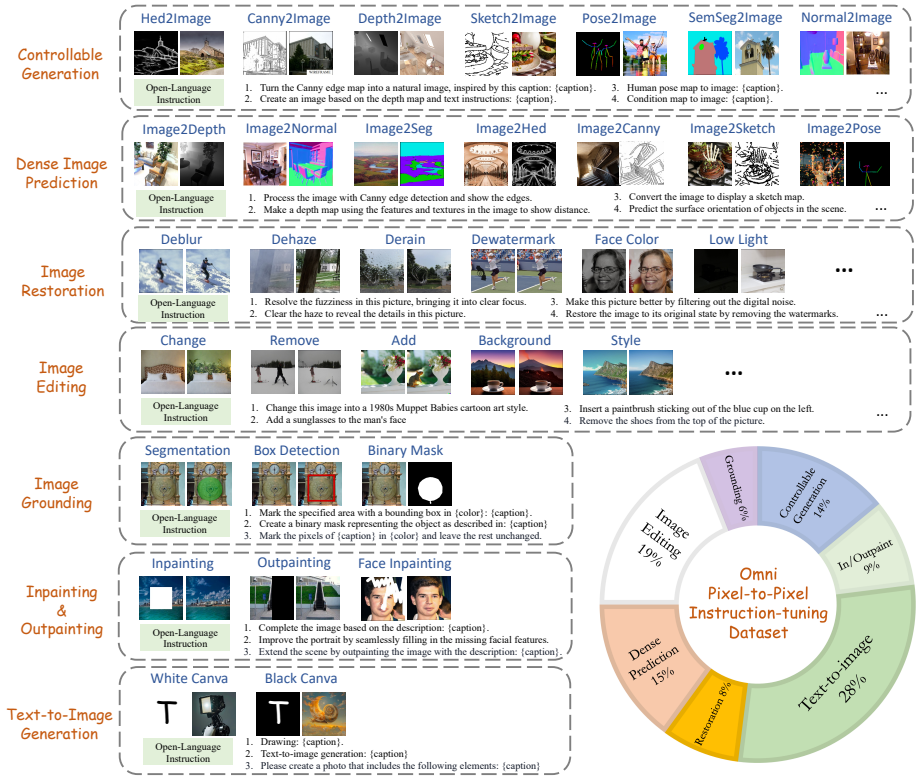

Figure 1: Task Overview of our Omni Pixel-to-Pixel Instruction-tuning Dataset for PixWizard.

• ***1. Task Unification:*** Given the diverse nature of vision tasks and data formats, ranging from pixels and coordinates to binary masks and categories, it is challenging to find a unified representation. We observe that most vision tasks can be framed as image-to-image translation problems. For tasks not naturally suited to image output, we first learn to generate their visualizations and then apply post-processing to convert them into the desired formats. This approach is a key step toward developing a versatile visual assistant.

• ***2. Data Construction:*** We aim to leverage and integrate the remarkable diversity of tasks and data in the visual domain. To achieve this, we have built a comprehensive training set with a total of 30 million data points, enabling our model to support five main capabilities: *(i)* Image generation, which includes text-to-image generation, controllable generation, inpainting, and outpainting; *(ii)* Image editing; *(iii)* Image restoration, covering tasks such as deraining, desnowing, deblurring, super-resolution, and more; *(iv)* Image grounding, which involves locating objects based on user prompts; and *(v)* Dense image prediction, which includes depth estimation, surface normal estimation, pose estimation, semantic segmentation, and image-to-canny/HED/sketch/Line-Art conversions.

• ***3. Architecture Design:*** For a robust visual assistant, the architecture and scalability of the foundation model are crucial. In this work, we use the flow-based Diffusion Transformer (DiT) (Ma et al., 2024), which offer great versatility and stability in modeling data distributions by learning conditional velocity fields. The DiT architecture further enhances scalability and is well-suited for incorporating conditional information. Building on this foundation, we introduce several key components. We extend the dynamic partitioning and padding scheme (Zhuo et al., 2024) to handle input images of any resolution, aligning closely with human perception. Additionally, we implement structure-aware and semantic-aware guidance, enabling the model to follow multimodal instructions (images and user prompts) for a wide range of manipulations.

Experimental results show that PixWizard achieves competitive performance on certain tasks compared to task-specific vision models, and outperforms current state-of-the-art general visual models in most tasks, delivering its strong overall multi-task performance. More importantly, our model handles tasks and instruction prompts it has not encountered during training, demonstrating impressive generalization capabilities. This further highlights PixWizard's strength as a powerful interactive image-to-image visual assistant.

2 OMNI PIXEL-TO-PIXEL INSTRUCTION-TUNING DATASET

To equip our image-to-image visual assistant with comprehensive capabilities in image generation, manipulation, and translation, we compiled a multi-task training dataset for visual instruction tuning, consisting of 30 million instances across seven primary domains, as illustrated in Fig. 1. To our knowledge, this is the largest and user-friendly image-instruction-image triplet dataset, built from both open-source and in-house data, filtered with the help of MLLMs and manual review.

Image Restoration. We incorporate low-level data to restore images degraded by various environmental or technical factors. This section utilizes a wide range of open-source datasets covering key restoration tasks, including *(1) Denoising*, *(2) Deraining*, *(3) Demoireing*, *(4) Dehazing*, *(5) Deblurring*, *(6) Desnowing*, *(7) Deshadowing*, *(8) Low-Light Enhancement*, *(9) Face Restoration*, *(10) Watermark Removal*, and *(11) Super Resolution*. Since both the inputs and outputs are inherently defined in the RGB space, these tasks can be seamlessly unified by our PixWizard model without any extra transformations. All open-source datasets we use are provided in Sec. B.1.

Image Grounding. Image grounding involves identifying and highlighting specific areas of objects in images based on provided text prompts. The data for this part is sourced from well-known datasets such as gRefCOCO (Liu et al., 2023a), RefCOCO3 (Yu et al., 2016), and Visual Genome (Krishna et al., 2017). We focus on three types of grounding tasks: *(1) Segmentation Referring*, where the target object specified by the user is highlighted in the output image; *(2) Box Detection Referring*, where the target object is highlighted using bounding boxes; and *(3) Binary Mask Prediction*, where a binary mask is directly predicted. (Details are provided in the Sec. B.2.)

Controllable Generation. Referring to ControlNet (Zhang et al., 2023a), we aim to equip our model with natural image generation capabilities given conditional inputs. We first gather natural images from the LAION Art dataset (Schuhmann et al., 2022) and our own collection of high-quality images from the Internet. We then use MiniCPM-Llama3-V 2.5 (Yao et al., 2024), a robust edge-side multimodal LLM, along with advanced techniques to generate captions and conditional inputs for the images. (Details on data construction can be found in Sec. B.3.)

Dense Image Prediction. Dense image prediction tasks require the model to interpret input images and produce dense annotations. For *depth estimation, surface normal estimation, and semantic segmentation*, we represent per-pixel labels as RGB images, which can be generated via the image generation capabilities. For other tasks, such as the prediction of *human pose maps*, *sketches*, *HED boundaries*, *canny edge maps*, and *cartoon line art*, we treat them as image-to-image translation tasks, as we can easily obtain image pairs using open-source tools. (Details are provided in the Sec. B.4.)

Image Editing. Instruction-based image editing holds great potential for practical applications, as it allows users to perform edits using natural language commands. To enhance our model's ability to modify images according to specific user instructions, we unify several public editing datasets, including UltraEdit (2024), MagicBrush (2024a), GQA-Inpaint (2023), Instruct P2P (2023), SEED-X-Edit (2024), GIER (2020), and HQ-Edit (2024). These datasets encompass a wide range of semantic entities, varying levels of detail, and multiple editing tasks including object removal, object replacement, object addition, background replacement, and style transfer.

Inpainting involves filling in missing parts of an image with new or modified content. To create inpainting instances, we apply random black or white masks to different regions of the original images. These masks come in various shapes, including circles, rectangles, and free-form patterns, and are randomly placed on the images, resulting in a wide range of occluded areas for inpainting.

Outpainting (Image extrapolation) extends an image's content beyond its boundaries. To create outpainting instances, we randomly crop the central part of the image, while masking the surrounding areas with black or white. The cropping is not limited to square shapes but includes rectangles of varying proportions. This approach ensures that the outpainting task covers a range of extension scenarios, challenging the model to generate coherent content beyond the original image boundaries.

Text-to-Image Generation. Image-to-image and text-to-image are distinct tasks: the former requires an additional input image as a condition, while the latter does not. Existing instruction-tuning methods adapt pretrained text-to-image models for image-to-image tasks, but often lose the original text-to-image capabilities. To unify both tasks within a single framework, we propose a "drawing" strategy that preserves text-to-image functionality. Specifically, we introduce an additional input—a fully white or black image—alongside language instructions. This simulates a blank canvas, allowing the

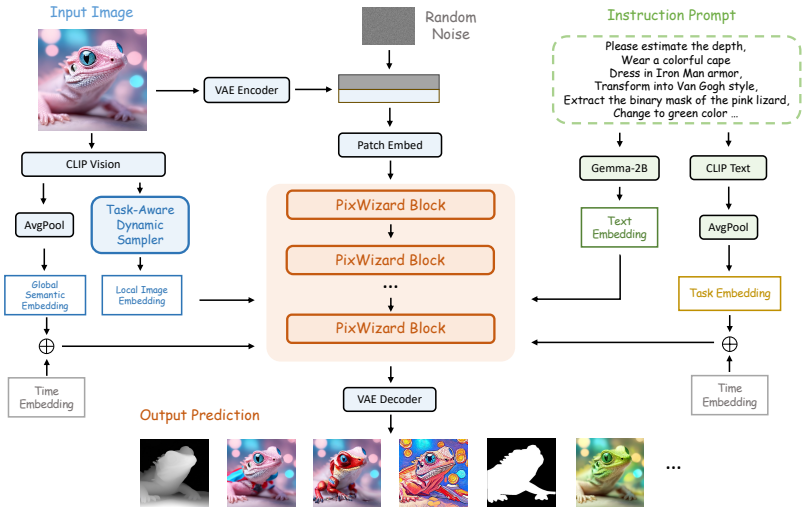

Figure 2: Overall framework of PixWizard.

model to "draw" images based on the text prompts. This approach differentiates our model from previous text-to-image systems. All image-text pairs are sourced from our collection of high-quality internet images, with captions generated using MLLM assistance.

Open-language Instruction. To enhance the usability of PixWizard as a practical visual assistant, we aim for the model to understand free-form user prompts. Instead of relying on fixed task-specific prompts, we begin by manually writing 6-10 prompts for each vision task to describe the task. We then use GPT-4o to generate a wide range of paraphrased variations. This process ensures that our instruction set remains diverse while staying true to the core intent of the original prompts. Instruction templates and examples are provided in Sec. B.5.

3 PIXWIZARD

PixWizard is a versatile image-to-image model fine-tuned on our custom-built omni pixel-to-pixel instruction-tuning dataset. In this section, we present the details of the PixWizard framework from the perspectives of model architecture (as shown in Fig. 2) and training strategies.

3.1 FLOW-BASED CONDITIONAL INSTRUCTION-TUNING

Previous studies (Wang et al., 2022b; Brooks et al., 2023) show that fine-tuning large diffusion models outperforms training models from scratch for image translation and editing tasks. Therefore, we initialize the weights of PixWizard with the pretrained Lumina-Next-T2I (Zhuo et al., 2024) checkpoint, which is a flow-based diffusion transformer, to leverage its extensive text-to-image generation capabilities. We learn a network v_θ that predicts the velocity field u_t given image conditioning c_I and text instruction conditioning c_T. We minimize the loss function as follow:

$$\mathcal{L} = \mathbb{E}_{t,p_1(x_1),p_t(x_t|x_1),c_I,c_T} \|v_\theta(x_t, t, c_I, c_T) - u_t(x_t, t|x_1)\|^2. \tag{1}$$

3.2 ARCHITECTURE

Text Encoders. We begin by using Gemma-2B (Team et al., 2024) as the text embedder in PixWizard to encode text prompts. However, in multi-task learning, relying solely on text instructions is insufficient to guide the model in accurately executing user commands. To better guide the generation process for the correct task, we incorporate the CLIP text encoder (Radford et al., 2021). Global average pooling is applied to the CLIP text embeddings to obtain a coarse-grained text representation, which is passed through an MLP-based task embedder to generate the task embedding. This embedding is then integrated into the PixWizard Block by adding it to the timestep embeddings through a modulation mechanism. In Sec. C.2, we show the t-SNE visualization to further illustrate the effectiveness of the task embedding.

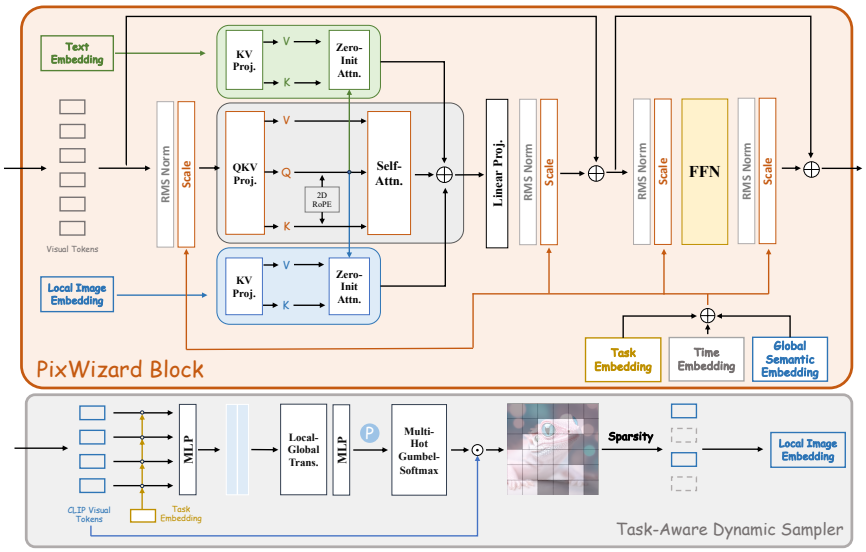

Figure 3: The schematic illustrations of PixWizard Block and Task-Aware Dynamic Sampler.

Structural-Aware Guidance. To effectively capture the overall structural features of the input image condition, we begin by encoding the image using a variational autoencoder (VAE) (Kingma & Welling, 2013) from SDXL (Podell et al., 2023). Next, we concatenate the image latent with the noise latent along the channel dimension (Saharia et al., 2022c;a). Following (Brooks et al., 2023), additional input channels are added to the patch embedder, with the weights for these new channels initially set to zero.

Semantic-Aware Guidance. Besides recognizing structural features, we use CLIP L/14-336 (Radford et al., 2021) to obtain semantic image embeddings. Within the PixWizard block, we introduce two zero-initialized attention mechanisms, allowing latent target image tokens to query information from the condition keys and values. Specifically, a zero-initialized gating mechanism is employed to gradually inject conditional image and text information into the token sequences. Given target image queries (Q_i), keys (K_i), and values (V_i), along with text instruction keys (K_t) and values (V_t), and conditional image keys (K_{ci}) and values (V_{ci}), the final attention output is formulated as:

$$A = \text{softmax}\left(\frac{\tilde{Q}_i \tilde{K}_i^T}{\sqrt{d}}\right) V_i + \tanh(\alpha_t)\,\text{softmax}\left(\frac{\tilde{Q}_i K_t^T}{\sqrt{d}}\right) V_t + \tanh(\alpha_{ci})\,\text{softmax}\left(\frac{\tilde{Q}_i K_{ci}^T}{\sqrt{d}}\right) V_{ci}, \tag{2}$$

where $\tilde{Q}_i$ and $\tilde{K}_i$ stand for applying RoPE (Su et al., 2024), d is the dimension of queries and keys, and α indicates the zero-initialized learnable parameter in gated cross-attention.

However, inputting all image tokens into the attention layer can lead to significant computational demands, and not all semantic tokens are relevant to the specific task. To address this, we introduce the Task-Aware Dynamic Sampler, designed to select the most relevant semantic tokens for each task. This sampler uses a lightweight ranking network with four linear layers and activation functions. Inspired by DynamicViT (Rao et al., 2021), we map image tokens to both local and global features. Additionally, task embeddings (x_{task}) are integrated to help the sampler identify the tokens most relevant to the task. The computational process is formulated as:

$$z = MLP(x + x_{task}) \in \mathbb{R}^{N \times C}, \tag{3}$$

$$z^{\text{local}} = z[:, : \frac{C}{2}] \in \mathbb{R}^{N \times \frac{C}{2}}, z^{\text{global}} = Avg(z[:, \frac{C}{2} :]) \in \mathbb{R}^{1 \times \frac{C}{2}}, z'_i = [z_i^{\text{local}}, z^{\text{global}}], \quad 1 \leq i \leq N, \tag{4}$$

$$M = MLP(z') \in \mathbb{R}^{N \times 1} \tag{5}$$

where M_i denotes the importance of the i-th token. However, implementing token sparsification is challenging in practice. Directly sampling tokens based on their importance scores is non-differentiable, which hinders end-to-end training. To address this, we use the Gumbel-Softmax technique (Jang et al., 2016) and adapt it into a Multi-Hot Gumbel-Softmax (MHGS) to enable simultaneous sampling of the top K tokens:

$$\hat{x} = x \odot MHGS(M) \tag{6}$$

Table 1: Comparison of PixWizard with task-specific and vision generalist baselines across six representative tasks, covering both high-level visual understanding and low-level image processing. '×' indicates that the method is incapable of performing the task.

Methods	Depth Est. RMSE↓		Semantic Seg. mIoU↑	Surface Normal Est. Mean Angle Error↓	Denoise PSNR↑	Denoise SSIM↑	Derain PSNR↑	Derain SSIM↑	Image Grounding cIoU↑ (val set)	
	NYUv2	SUNRGB-D	ADE20K	NYU-Depth V2	SIDD		Rain100L		RefCOCO	RefCOCO+
DepthAnything (2024a)	0.206	-								
Marigold (2024a)	0.224	-								
Mask DINO (2023)			60.80							
Mask2Former (2022)			56.10							
Bae et al. (2021)				14.90						
InvPT (2022)				19.04						
AirNet (2022)					38.32	0.945	32.98	0.951		
PromptIR (2024)					39.52	0.954	36.37	0.972		
LAVT (2022)									72.73	56.86
ReLA (2023a)									73.21	56.10
Unified-IO (2022b)	0.387	0.287	25.71	-	×	×	×	×	46.42	**40.50**
Painter (2023b)	0.288	0.285	**49.90**	×	**38.71**	0.954	29.87	0.882	×	×
InstructCV (2024)	0.297	**0.279**	47.23	×	×	×	×	×	×	×
InstructDiffusion (2024)	×	×	×	×	34.26	0.938	19.82	0.741	41.64*	33.20*
PixWizard	**0.287**	0.288	36.76	**19.65**	38.67	**0.957**	**31.43**	**0.917**	**46.44**	36.49

where the output of GumbelSoftmax is a multi-hot tensor representing the mask of the retained tokens. $\odot$ denotes the Hadamard product, where the top K tokens by importance score are weighted by 1 and retained, while the remaining $(N - K)$ tokens are weighted by zero and discarded. Each layer is equipped with an independent task-aware dynamic sampler. This approach not only captures the most relevant semantic features needed by each layer for different tasks but also reduces the computational cost in the attention process.

3.3 Two-Stage Training and Data Balancing Strategies

To unlock the model's potential and improve its performance on tasks with smaller datasets, we propose a two-stage training and data-balancing strategy. **S1:** In the first stage, we initialize the model by combining the weights of a pre-trained Lumina-Next-T2I (Zhuo et al., 2024) with randomly initialized weights for the newly added modules. We prioritize tasks with smaller datasets, assigning each a sampling weight to increase its data volume. This weight determines how many times the dataset is repeated during an epoch. Using this method, each task achieves approximately 20k data points. We then randomly sample from other tasks to match this scale, creating our first-stage training dataset, with training spanning 4 epochs. **S2:** In the second stage, we initialize the model using the weights from the first stage and combine all the collected data for further training. To balance tasks, we assign manual sampling weights to each dataset, randomly selecting data when a weight is less than 1.0. We also include text-to-image data at a 1:1 ratio with other tasks, resulting in a second-stage training dataset. At this stage, the total dataset reaches up to 20 million samples.

4 Experiments

4.1 First Section Results

Settings. For image restoration, we follow previous works (Conde et al., 2024; Potlapalli et al., 2024) and prepare datasets for various restoration tasks during training. For evaluation, we first select two representative benchmarks: Rain100L (2017) for deraining and SIDD (2018) for denoising. Additionally, we further assess performance on other restoration tasks and evaluate zero-shot capabilities in the Sec. D.2.

For image grounding, we evaluate referring segmentation tasks on the gRefCOCO (2023a), RefCOCO, and RefCOCO+ validation and test sets. To assess the performance gap with specialized models, we report results from several expert methods and primarily compare our approach with two unified models: Unified-IO and InstructDiffusion. Following standard practices (Liu et al., 2023a), we use cumulative IoU (cIoU) as the performance metric.

Dense image prediction tasks are evaluated across three vision tasks: ADE20k (2017b) for semantic segmentation, NYUv2 (2012) and SUNRGB-D (2014) for monocular depth estimation, and NYU-Depth v2 (2012) for surface normal estimation. Implementation details can be found in Sec. D.1.

Results. Table 1 presents a comprehensive performance comparison with recent state-of-the-art (SOTA) task-specific and all-in-one methods. As shown in the results, despite denoising and deraining

data making up only a small portion of the overall training set, our method outperforms other unified methods and even surpasses some task-specific approaches. In the image grounding task, PixWizard significantly outperforms the diffusion-based generalist model InstructDiffusion by 4.8 cIoU on RefCOCO (val). However, there is still room for improvement compared to other highly specialized models. Furthermore, as shown in Fig.5, PixWizard supports flexible instructions, allowing it to highlight and visualize the target object directly on the image while also generating the corresponding binary mask. This demonstrates its strong performance in real-world interactions and practical applications. Additional quantitative evaluation results are provided in the Sec. D.3.

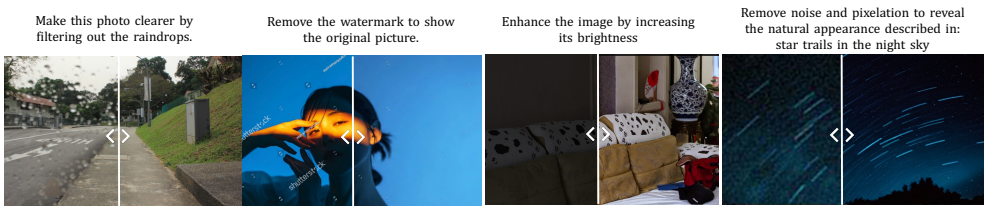

Figure 4: Qualitative Evaluation of Instruction-based Image Restoration.

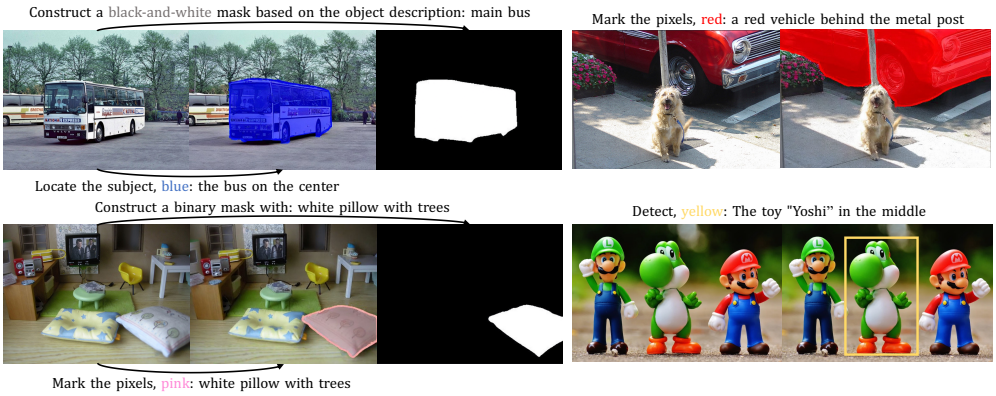

Figure 5: Qualitative Results of Instruction-based Image Grounding.

For dense prediction tasks, PixWizard performs competitively against both generalist and task-specific baselines across all three tasks. In depth estimation on the NYUv2 test set, PixWizard achieves a 10.0% improvement in RMSE compared to Unified-IO and performs similarly to Painter and InstructCV. For semantic segmentation, PixWizard surpasses Unified-IO by +11.05 in mIoU, though it still trails behind other methods. Additionally, Fig. 6 provides examples of PixWizard's outputs. As shown, by supplying the corresponding task-specific prompt for the same image, we can easily generate the respective condition visualization, underscoring PixWizard's significant practical value.

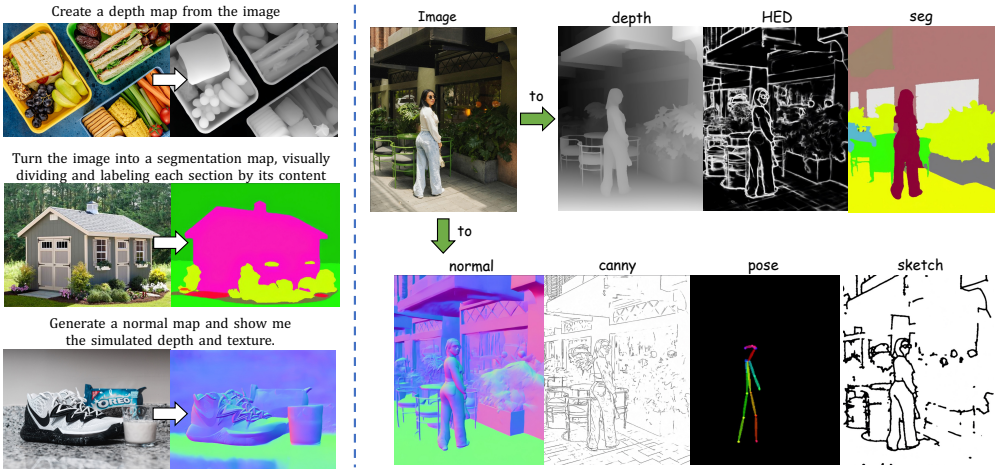

Figure 6: Visualizations of dense image prediction examples.

4.2 SECOND SECTION RESULTS (IMAGE EDITING)

Settings. We evaluate PixWizard across two benchmarks, the MagicBrush Test (Zhang et al., 2024a) and the Emu Edit Test (Sheynin et al., 2024), to assess its effectiveness in image editing capabilities. For a fair comparison, we primarily compare it with instruction-guided image editing methods, including InstructPix2Pix, MagicBrush, Emu Edit, and UltraEdit. Consistent with Emu Edit, we use L1 distance, CLIP image similarity, DINO similarity, CLIP text-image similarity, and CLIP text-image direction similarity as metrics.

Table 2: Comparison with image-editing baselines evaluated on Emu Edit and MagicBrush test set.

	Emu Edit Test set					MagicBrush Test Set				
Method	$\text{CLIP}_{dir}\uparrow$	$\text{CLIP}_{im}\uparrow$	$\text{CLIP}_{out}\uparrow$	L1↓	DINO↑	$\text{CLIP}_{dir}\uparrow$	$\text{CLIP}_{im}\uparrow$	$\text{CLIP}_{out}\uparrow$	L1↓	DINO↑
InstructPix2Pix (2023)	0.078	0.834	0.219	0.121	0.762	0.115	0.837	0.245	0.093	0.767
MagicBrush (2024a)	0.090	0.838	0.222	0.100	0.776	0.123	0.883	0.261	0.058	0.871
Emu Edit (2024)	**0.109**	**0.859**	0.231	0.094	**0.819**	**0.135**	**0.897**	0.261	**0.052**	**0.879**
UltraEdit (2024)	0.107	0.844	**0.283**	0.071	0.793	-	0.868	-	0.088	0.792
PixWizard	0.104	0.845	0.248	**0.069**	0.798	0.124	0.884	**0.265**	0.063	0.876

Figure 7: Qualitative examples comparing PixWizard with other editing approaches.

Results. Table 2 presents our results compared to the baselines. The findings show that our model consistently outperforms InstructPix2Pix, MagicBrush, and UltraEdit in automatic metrics and achieves comparable performance to state-of-the-art method Emu Edit. Qualitative comparisons are provided in Fig. 7. Our model precisely identifies the editing region while preserving the rest of the pixels, and it demonstrates the best understanding of the given instructions.

4.3 THIRD SECTION RESULTS (IMAGE GENERATION)

In this section, we focus on evaluating the effectiveness of PixWizard's generation capabilities. Specifically, we assess its performance across four tasks: text-to-image generation, controllable image generation, inpainting, and outpainting. Implementation details can be found in Sec. D.1.

Controllable Generation Results. Without the need for separate training for each model, PixWizard is an all-in-one solution capable of handling multiple conditions. As shown in Table 3 and Fig. 8, PixWizard achieves the highest controllability and best image quality under depth conditions, while also being comparable to current separate models in image-text alignment.

Inpainting Results. As shown in Table 3, PixWizard outperforms other inpainting approaches, improving overall image quality based on FID and LPIPS scores. The qualitative examples in Fig. 9 further demonstrate PixWizard's effectiveness in generating coherent content. Building on its strong inpainting capabilities, PixWizard enables users to perform more precise image editing tasks, such as *Remove Anything*, *Replace Anything*, and *Add Anything*. More details can be found in Sec. D.4

Outpainting Results. As shown in the quantitative comparison results in Table 3, PixWizard outperforms other baselines in the outpainting task, delivering state-of-the-art image generation

Table 3: Comparison of PixWizard with task-specific baselines across five representative tasks.

Methods	Canny-to-Image			Depth-to-Image			Inpainting		Outpainting		Text-to-Image	
	FI↑	FID↓	CLIP-S↑	RMSE↓	FID↓	CLIP-S↑	FID↓	LPIPS↓	FID↓	IS↑	FID↓	HPSv2↑
	MultiGen-20M			MultiGen-20M			Places		Places		COCO-30K	Photo
ControlNet-SD1.5 (2023a)	34.65	14.73	**32.15**	35.90	17.76	**32.45**						
T2I-Adapter-SD1.5 (2024)	23.65	**15.96**	31.71	48.40	22.52	31.46						
LDM-4 (2022b)							9.39	0.246				
LaMa (2022)							12.0	**0.24**				
DeepFill v2 (2019)									11.51	17.70		
MaskGIT (2022b)									7.80	**22.95**		
DALL·E 2 (2021)											10.32	27.24 ± 0.198
SD 1.5 (2022b)											9.62	27.46 ± 0.198
PixArt-α (2024b)											**7.32**	-
Lumina-Next (2024)											9.79	27.47 ± 0.203
PixWizard	**35.46**	15.76	32.01	**33.83**	**16.94**	31.84	**9.27**	0.25	**7.54**	22.18	9.56	**27.47 ± 0.183**

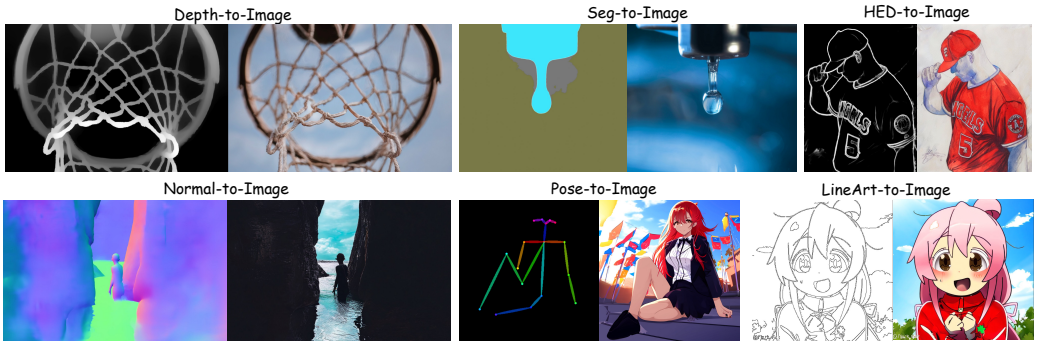

Figure 8: Visualization examples under different conditions.

quality with a FID score of 7.54 and an IS score of 22.18. The samples in Fig. 9 demonstrate PixWizard's ability to synthesize images in various scenes and styles, and it flexibly handles image extrapolation in multiple directions and aspect ratios with better marginal coherence.

Text-to-Image Results. As the results shown in Table 3, PixWizard achieves a FID score of 9.56 when tested for zero-shot performance on the COCO dataset. Although some models achieve a lower FID, they focus solely on text-to-image tasks and rely on significantly more training resources. Additionally, we evaluated the Human Preference Score (HPS v2), a robust benchmark for assessing human preferences in text-to-image synthesis. PixWizard performed well, delivering image quality comparable to popular text-to-image generators. We provide visual samples in Fig. 9. PixWizard supports high-resolution image synthesis, up to 1024×1024, with any resolution and aspect ratio.

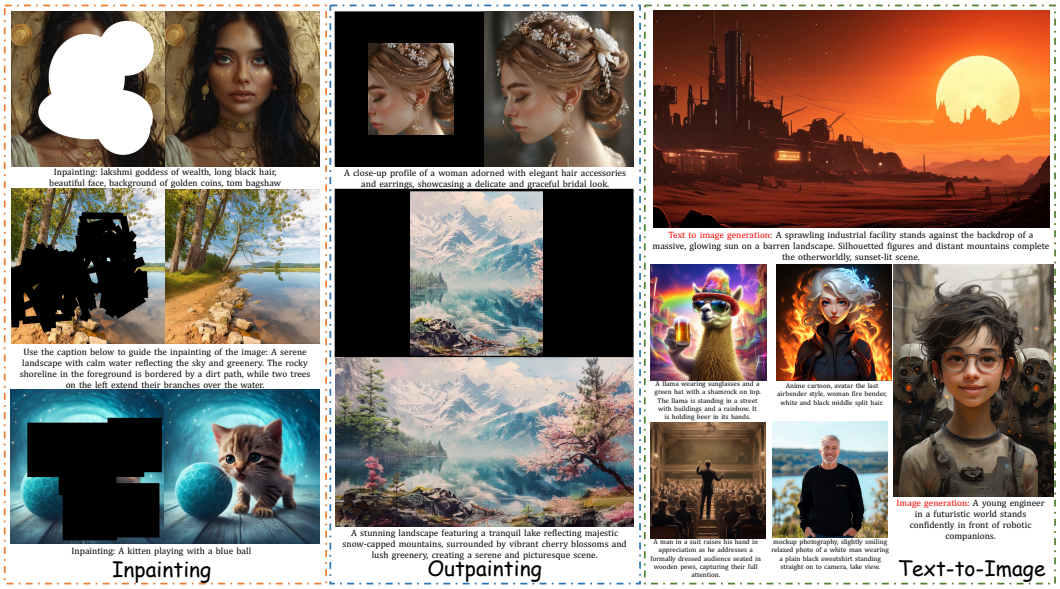

Figure 9: Visualization results of **Inpainting**, **Outpainting** and **Text-to-Image Generation**.

4.4 Ablation Study

We performed ablation studies to assess the impact of each component's design and the training process on learning in PixWizard. Given computational limitations, we conducted the ablation on PixWizard, training it for 40k steps.

Table 4: Comparison of the models with two different guidances, dynamic semantic tokens sampling (DSTS), and two-stage training and data balancing strategy for different tasks.

Methods	**Deraining** Rain100L	**RefCOCO** val	**Depth Estim.** NYUv2	**Image Editing** Emu Edit	**Canny-to-Image** MultiGen-20M		**Inpainting** Places
	PSNR↑	cIoU↑	RMSE↓	CLIP_{dir}↑	F1↑	FID↓	FID↓
M1	$29.91_{(-0.33)}$	$40.78_{(-0.94)}$	$0.319_{(+0.005)}$	$0.078_{(-0.010)}$	$32.98_{(-0.03)}$	$17.41_{(-0.27)}$	$10.91_{(-0.03)}$
M2	$14.72_{(-15.52)}$	$18.43_{(-23.29)}$	$0.586_{(-0.262)}$	$0.071_{(-0.017)}$	$11.12_{(-23.89)}$	$19.34_{(-2.20)}$	$13.87_{(-2.99)}$
PixWizard w/o DSTS	$30.19_{(-0.05)}$	$41.66_{(-0.06)}$	$0.318_{(+0.006)}$	$0.091_{(+0.003)}$	$32.93_{(-0.08)}$	$17.02_{(+0.12)}$	$10.93_{(-0.05)}$
PixWizard w/o two-stage	$29.17_{(-1.07)}$	$40.18_{(-1.54)}$	$0.322_{(+0.002)}$	$0.085_{(-0.003)}$	$32.87_{(-0.14)}$	$17.21_{(-0.07)}$	$10.97_{(-0.09)}$
PixWizard	30.24	41.72	0.324	0.088	33.01	17.14	10.88

Structural-Aware vs. Semantic-Aware Guidance. We demonstrate the importance of integrating both structure-aware and semantic-aware guidance to enhance PixWizard's performance across diverse tasks. To validate this, we trained two additional models: $M1$ with only the structure-aware module and $M2$ with only the semantic-aware module. Results show that $M1$ performs better on tasks requiring preservation of image structure and details, while $M2$, which relies solely on cross-attention for injecting image features, struggles with most visual tasks and often generates outputs that deviate from the input. However, as noted by other methods (Ye et al., 2023; Hu et al., 2024), semantic guidance excels in tasks needing flexibility, such as text-to-image generation, conditional generation, and image editing. In comparison, PixWizard, which combines both modules, achieves balanced performance across a broader range of tasks.

Influence of Dynamic Semantic Tokens Sampling. As shown in Table 4, the impact of Dynamic Semantic Tokens Sampling (DSTS) on task performance is minimal, but it improves overall performance on average. This indicates that modeling semantic tokens for the entire image is unnecessary. By dynamically sampling relevant features for each task's focus, the model operates more efficiently. Moreover, using fewer tokens reduces computational load during attention calculations, resulting in faster inference.

Influence of Two-Stage Training and Data Balancing. Table 4 presents the results of our proposed two-stage training and data balancing strategy. As shown, our approach is crucial, as the two-stage method significantly improves performance on tasks with smaller datasets while maintaining the same number of training steps and achieving faster convergence. Notably, for tasks with larger datasets, the performance remains comparable.

5 Discussion and Conclusion

In this work, we explore how to build a versatile interactive image-to-image visual assistant from three key aspects: task definition, data construction, and model architecture. Our goal is to create a system that can precisely follow free-form user instructions for image generation, manipulation, and translation. Our PixWizard eliminates the need for task-specific design choices and achieves highly competitive performance across a diverse set of tasks, with strong generalization capabilities.

However, this work has some limitations. First, the current model architecture does not yet support multi-image input conditions, which is an increasingly important research area. Second, there is room for improvement in challenging tasks like segmentation and image grounding compared to specialized models. Additionally, the performance of the text encoder and foundation model also plays a crucial role. Better text encoding improves the model's ability to understand and execute instructions, while larger, more robust architectures enhance output quality. Notably, the modules and strategies proposed in PixWizard can be easily applied to other powerful text-to-image generators. In the future, we plan to explore more advanced diffusion models, such as SD3 and FLUX, and continue advancing this field toward a "GPT-4 moment".

REFERENCES

Abdelrahman Abdelhamed, Stephen Lin, and Michael S Brown. A high-quality denoising dataset for smartphone cameras. In *Proceedings of the IEEE conference on computer vision and pattern recognition*, pp. 1692–1700, 2018.

Abdullah Abuolaim and Michael S Brown. Defocus deblurring using dual-pixel data. In *Computer Vision–ECCV 2020: 16th European Conference, Glasgow, UK, August 23–28, 2020, Proceedings, Part X 16*, pp. 111–126. Springer, 2020.

Josh Achiam, Steven Adler, Sandhini Agarwal, Lama Ahmad, Ilge Akkaya, Florencia Leoni Aleman, Diogo Almeida, Janko Altenschmidt, Sam Altman, Shyamal Anadkat, et al. Gpt-4 technical report. *arXiv preprint arXiv:2303.08774*, 2023.

Eirikur Agustsson and Radu Timofte. Ntire 2017 challenge on single image super-resolution: Dataset and study. In *Proceedings of the IEEE conference on computer vision and pattern recognition workshops*, pp. 126–135, 2017.

Yuang Ai, Huaibo Huang, Xiaoqiang Zhou, Jiexiang Wang, and Ran He. Multimodal prompt perceiver: Empower adaptiveness generalizability and fidelity for all-in-one image restoration. In *Proceedings of the IEEE/CVF Conference on Computer Vision and Pattern Recognition*, pp. 25432–25444, 2024.

Michael Samuel Albergo and Eric Vanden-Eijnden. Building normalizing flows with stochastic interpolants. In *The Eleventh International Conference on Learning Representations*, 2023. URL https://openreview.net/forum?id=li7qeBbCR1t.

Codruta O Ancuti, Cosmin Ancuti, Mateu Sbert, and Radu Timofte. Dense-haze: A benchmark for image dehazing with dense-haze and haze-free images. In *2019 IEEE international conference on image processing (ICIP)*, pp. 1014–1018. IEEE, 2019.

Codruta O Ancuti, Cosmin Ancuti, and Radu Timofte. Nh-haze: An image dehazing benchmark with non-homogeneous hazy and haze-free images. In *Proceedings of the IEEE/CVF conference on computer vision and pattern recognition workshops*, pp. 444–445, 2020.

Omri Avrahami, Dani Lischinski, and Ohad Fried. Blended diffusion for text-driven editing of natural images. In *Proceedings of the IEEE/CVF conference on computer vision and pattern recognition*, pp. 18208–18218, 2022.

Roman Bachmann, Oğuzhan Fatih Kar, David Mizrahi, Ali Garjani, Mingfei Gao, David Griffiths, Jiaming Hu, Afshin Dehghan, and Amir Zamir. 4m-21: An any-to-any vision model for tens of tasks and modalities. *arXiv preprint arXiv:2406.09406*, 2024.

Gwangbin Bae and Andrew J. Davison. Rethinking inductive biases for surface normal estimation. In *IEEE/CVF Conference on Computer Vision and Pattern Recognition (CVPR)*, 2024.

Gwangbin Bae, Ignas Budvytis, and Roberto Cipolla. Estimating and exploiting the aleatoric uncertainty in surface normal estimation. In *Proceedings of the IEEE/CVF International Conference on Computer Vision*, pp. 13137–13146, 2021.

Yutong Bai, Xinyang Geng, Karttikeya Mangalam, Amir Bar, Alan L Yuille, Trevor Darrell, Jitendra Malik, and Alexei A Efros. Sequential modeling enables scalable learning for large vision models. In *Proceedings of the IEEE/CVF Conference on Computer Vision and Pattern Recognition*, pp. 22861–22872, 2024.

Dmitry Baranchuk, Andrey Voynov, Ivan Rubachev, Valentin Khrulkov, and Artem Babenko. Label-efficient semantic segmentation with diffusion models. In *International Conference on Learning Representations*, 2022. URL https://openreview.net/forum?id=SlxSY2UZQT.

James Betker, Gabriel Goh, Li Jing, Tim Brooks, Jianfeng Wang, Linjie Li, Long Ouyang, Juntang Zhuang, Joyce Lee, Yufei Guo, et al. Improving image generation with better captions. *Computer Science. https://cdn. openai. com/papers/dall-e-3. pdf*, 2(3):8, 2023.

Tim Brooks, Aleksander Holynski, and Alexei A Efros. Instructpix2pix: Learning to follow image editing instructions. In *Proceedings of the IEEE/CVF Conference on Computer Vision and Pattern Recognition*, pp. 18392–18402, 2023.

Tim Brooks, Bill Peebles, Connor Holmes, Will DePue, Yufei Guo, Li Jing, David Schnurr, Joe Taylor, Troy Luhman, Eric Luhman, Clarence Ng, Ricky Wang, and Aditya Ramesh. Video generation models as world simulators. 2024. URL https://openai.com/research/video-generation-models-as-world-simulators.

Tom Brown, Benjamin Mann, Nick Ryder, Melanie Subbiah, Jared D Kaplan, Prafulla Dhariwal, Arvind Neelakantan, Pranav Shyam, Girish Sastry, Amanda Askell, et al. Language models are few-shot learners. *Advances in Neural Information Processing Systems*, 33:1877–1901, 2020.

Yohann Cabon, Naila Murray, and Martin Humenberger. Virtual kitti 2. *arXiv preprint arXiv:2001.10773*, 2020.

Jianrui Cai, Hui Zeng, Hongwei Yong, Zisheng Cao, and Lei Zhang. Toward real-world single image super-resolution: A new benchmark and a new model. In *Proceedings of the IEEE International Conference on Computer Vision*, 2019.

John Canny. A computational approach to edge detection. *IEEE Transactions on pattern analysis and machine intelligence*, (6):679–698, 1986.

Zhe Cao, Tomas Simon, Shih-En Wei, and Yaser Sheikh. Realtime multi-person 2d pose estimation using part affinity fields. In *Proceedings of the IEEE conference on computer vision and pattern recognition*, pp. 7291–7299, 2017.

Mathilde Caron, Hugo Touvron, Ishan Misra, Hervé Jégou, Julien Mairal, Piotr Bojanowski, and Armand Joulin. Emerging properties in self-supervised vision transformers. In *Proceedings of the IEEE/CVF international conference on computer vision*, pp. 9650–9660, 2021.

Huiwen Chang, Han Zhang, Lu Jiang, Ce Liu, and William T Freeman. Maskgit: Masked generative image transformer. In *Proceedings of the IEEE/CVF Conference on Computer Vision and Pattern Recognition*, pp. 11315–11325, 2022a.

Huiwen Chang, Han Zhang, Lu Jiang, Ce Liu, and William T Freeman. Maskgit: Masked generative image transformer. In *Proceedings of the IEEE/CVF Conference on Computer Vision and Pattern Recognition*, pp. 11315–11325, 2022b.

Junsong Chen, Chongjian Ge, Enze Xie, Yue Wu, Lewei Yao, Xiaozhe Ren, Zhongdao Wang, Ping Luo, Huchuan Lu, and Zhenguo Li. Pixart-\sigma: Weak-to-strong training of diffusion transformer for 4k text-to-image generation. *arXiv preprint arXiv:2403.04692*, 2024a.

Junsong Chen, Jincheng YU, Chongjian GE, Lewei Yao, Enze Xie, Zhongdao Wang, James Kwok, Ping Luo, Huchuan Lu, and Zhenguo Li. Pixart-α: Fast training of diffusion transformer for photorealistic text-to-image synthesis. In *The Twelfth International Conference on Learning Representations*, 2024b. URL https://openreview.net/forum?id=eAKmQPe3m1.

Liangyu Chen, Xiaojie Chu, Xiangyu Zhang, and Jian Sun. Simple baselines for image restoration. In *European conference on computer vision*, pp. 17–33. Springer, 2022a.

Ricky TQ Chen, Yulia Rubanova, Jesse Bettencourt, and David K Duvenaud. Neural ordinary differential equations. *Advances in neural information processing systems*, 31, 2018.

Ting Chen, Saurabh Saxena, Lala Li, Tsung-Yi Lin, David J Fleet, and Geoffrey E Hinton. A unified sequence interface for vision tasks. *Advances in Neural Information Processing Systems*, 35: 31333–31346, 2022b.

Bowen Cheng, Ishan Misra, Alexander G Schwing, Alexander Kirillov, and Rohit Girdhar. Masked-attention mask transformer for universal image segmentation. In *Proceedings of the IEEE/CVF conference on computer vision and pattern recognition*, pp. 1290–1299, 2022.

Marcos V Conde, Gregor Geigle, and Radu Timofte. High-quality image restoration following human instructions. *arXiv preprint arXiv:2401.16468*, 2024.

Antonio Criminisi, Patrick Perez, and Kentaro Toyama. Object removal by exemplar-based inpainting. In *2003 IEEE Computer Society Conference on Computer Vision and Pattern Recognition, 2003. Proceedings.*, volume 2, pp. II–II. IEEE, 2003.

Antonio Criminisi, Patrick Pérez, and Kentaro Toyama. Region filling and object removal by exemplar-based image inpainting. *IEEE Transactions on image processing*, 13(9):1200–1212, 2004.

Prafulla Dhariwal and Alexander Nichol. Diffusion models beat gans on image synthesis. *Advances in neural information processing systems*, 34:8780–8794, 2021.

Runpei Dong, Chunrui Han, Yuang Peng, Zekun Qi, Zheng Ge, Jinrong Yang, Liang Zhao, Jianjian Sun, Hongyu Zhou, Haoran Wei, Xiangwen Kong, Xiangyu Zhang, Kaisheng Ma, and Li Yi. DreamLLM: Synergistic multimodal comprehension and creation. In *The Twelfth International Conference on Learning Representations*, 2024. URL https://openreview.net/forum?id=y01KGvd9Bw.

Omar Elharrouss, Noor Almaadeed, Somaya Al-Maadeed, and Younes Akbari. Image inpainting: A review. *Neural Processing Letters*, 51:2007–2028, 2020.

Patrick Esser, Robin Rombach, and Bjorn Ommer. Taming transformers for high-resolution image synthesis. In *Proceedings of the IEEE/CVF conference on computer vision and pattern recognition*, pp. 12873–12883, 2021.

Patrick Esser, Sumith Kulal, Andreas Blattmann, Rahim Entezari, Jonas Müller, Harry Saini, Yam Levi, Dominik Lorenz, Axel Sauer, Frederic Boesel, et al. Scaling rectified flow transformers for high-resolution image synthesis. In *Forty-first International Conference on Machine Learning*, 2024.

Xueyang Fu, Jiabin Huang, Delu Zeng, Yue Huang, Xinghao Ding, and John Paisley. Removing rain from single images via a deep detail network. In *Proceedings of the IEEE conference on computer vision and pattern recognition*, pp. 3855–3863, 2017.

Yulu Gan, Sungwoo Park, Alexander Marcel Schubert, Anthony Philippakis, and Ahmed Alaa. InstructCV: Instruction-tuned text-to-image diffusion models as vision generalists. In *The Twelfth International Conference on Learning Representations*, 2024. URL https://openreview.net/forum?id=Nu9mOSq7eH.

Peng Gao, Renrui Zhang, Chris Liu, Longtian Qiu, Siyuan Huang, Weifeng Lin, Shitian Zhao, Shijie Geng, Ziyi Lin, Peng Jin, et al. Sphinx-x: Scaling data and parameters for a family of multi-modal large language models. *ICML 2024*, 2024.

Yuying Ge, Sijie Zhao, Chen Li, Yixiao Ge, and Ying Shan. Seed-data-edit technical report: A hybrid dataset for instructional image editing. *arXiv preprint arXiv:2405.04007*, 2024.

Zigang Geng, Binxin Yang, Tiankai Hang, Chen Li, Shuyang Gu, Ting Zhang, Jianmin Bao, Zheng Zhang, Houqiang Li, Han Hu, et al. Instructdiffusion: A generalist modeling interface for vision tasks. In *Proceedings of the IEEE/CVF Conference on Computer Vision and Pattern Recognition*, pp. 12709–12720, 2024.

Ziyu Guo, Renrui Zhang, Xiangyang Zhu, Yiwen Tang, Xianzheng Ma, Jiaming Han, Kexin Chen, Peng Gao, Xianzhi Li, Hongsheng Li, et al. Point-bind & point-llm: Aligning point cloud with multi-modality for 3d understanding, generation, and instruction following. *arXiv preprint arXiv:2309.00615*, 2023.

Ziyu Guo, Renrui Zhang, Xiangyang Zhu, Chengzhuo Tong, Peng Gao, Chunyuan Li, and Pheng-Ann Heng. Sam2point: Segment any 3d as videos in zero-shot and promptable manners. *arXiv preprint arXiv:2408.16768*, 2024.

Jiaming Han, Renrui Zhang, Wenqi Shao, Peng Gao, Peng Xu, Han Xiao, Kaipeng Zhang, Chris Liu, Song Wen, Ziyu Guo, et al. Imagebind-llm: Multi-modality instruction tuning. *arXiv preprint arXiv:2309.03905*, 2023.

Jonathan Ho and Tim Salimans. Classifier-free diffusion guidance. *arXiv preprint arXiv:2207.12598*, 2022.

Jonathan Ho, Ajay Jain, and Pieter Abbeel. Denoising diffusion probabilistic models. *Advances in neural information processing systems*, 33:6840–6851, 2020.

Jonathan Ho, Tim Salimans, Alexey Gritsenko, William Chan, Mohammad Norouzi, and David J Fleet. Video diffusion models. *Advances in Neural Information Processing Systems*, 35:8633–8646, 2022.

Hexiang Hu, Kelvin CK Chan, Yu-Chuan Su, Wenhu Chen, Yandong Li, Kihyuk Sohn, Yang Zhao, Xue Ben, Boqing Gong, William Cohen, et al. Instruct-imagen: Image generation with multi-modal instruction. In *Proceedings of the IEEE/CVF Conference on Computer Vision and Pattern Recognition*, pp. 4754–4763, 2024.

Huaibo Huang, Mandi Luo, and Ran He. Memory uncertainty learning for real-world single image deraining. *IEEE Transactions on Pattern Analysis and Machine Intelligence*, 45(3):3446–3460, 2022.

Rongjie Huang, Jiawei Huang, Dongchao Yang, Yi Ren, Luping Liu, Mingze Li, Zhenhui Ye, Jinglin Liu, Xiang Yin, and Zhou Zhao. Make-an-audio: Text-to-audio generation with prompt-enhanced diffusion models. In *International Conference on Machine Learning*, pp. 13916–13932. PMLR, 2023.

Mude Hui, Siwei Yang, Bingchen Zhao, Yichun Shi, Heng Wang, Peng Wang, Yuyin Zhou, and Cihang Xie. Hq-edit: A high-quality dataset for instruction-based image editing. *arXiv preprint arXiv:2404.09990*, 2024.

Jitesh Jain, Jiachen Li, Mang Tik Chiu, Ali Hassani, Nikita Orlov, and Humphrey Shi. Oneformer: One transformer to rule universal image segmentation. In *Proceedings of the IEEE/CVF Conference on Computer Vision and Pattern Recognition*, pp. 2989–2998, 2023.

Eric Jang, Shixiang Gu, and Ben Poole. Categorical reparameterization with gumbel-softmax. *arXiv preprint arXiv:1611.01144*, 2016.

Dongzhi Jiang, Guanglu Song, Xiaoshi Wu, Renrui Zhang, Dazhong Shen, Zhuofan Zong, Yu Liu, and Hongsheng Li. Comat: Aligning text-to-image diffusion model with image-to-text concept matching. *arXiv preprint arXiv:2404.03653*, 2024a.

Dongzhi Jiang, Renrui Zhang, Ziyu Guo, Yanmin Wu, Jiayi Lei, Pengshuo Qiu, Pan Lu, Zehui Chen, Guanglu Song, Peng Gao, et al. Mmsearch: Benchmarking the potential of large models as multi-modal search engines. *arXiv preprint arXiv:2409.12959*, 2024b.

Tero Karras, Samuli Laine, and Timo Aila. A style-based generator architecture for generative adversarial networks. In *Proceedings of the IEEE/CVF conference on computer vision and pattern recognition*, pp. 4401–4410, 2019.

Bahjat Kawar, Shiran Zada, Oran Lang, Omer Tov, Huiwen Chang, Tali Dekel, Inbar Mosseri, and Michal Irani. Imagic: Text-based real image editing with diffusion models. In *Proceedings of the IEEE/CVF Conference on Computer Vision and Pattern Recognition*, pp. 6007–6017, 2023.

Bingxin Ke, Anton Obukhov, Shengyu Huang, Nando Metzger, Rodrigo Caye Daudt, and Konrad Schindler. Repurposing diffusion-based image generators for monocular depth estimation. In *Proceedings of the IEEE/CVF Conference on Computer Vision and Pattern Recognition*, pp. 9492–9502, 2024a.

Bingxin Ke, Anton Obukhov, Shengyu Huang, Nando Metzger, Rodrigo Caye Daudt, and Konrad Schindler. Repurposing diffusion-based image generators for monocular depth estimation. In *Proceedings of the IEEE/CVF Conference on Computer Vision and Pattern Recognition*, pp. 9492–9502, 2024b.

Diederik P Kingma and Max Welling. Auto-encoding variational bayes. *arXiv preprint arXiv:1312.6114*, 2013.

Jing Yu Koh, Daniel Fried, and Russ R Salakhutdinov. Generating images with multimodal language models. *Advances in Neural Information Processing Systems*, 36, 2024.

Zhifeng Kong, Wei Ping, Jiaji Huang, Kexin Zhao, and Bryan Catanzaro. Diffwave: A versatile diffusion model for audio synthesis. In *International Conference on Learning Representations*, 2021. URL https://openreview.net/forum?id=a-xFK8Ymz5J.

Ranjay Krishna, Yuke Zhu, Oliver Groth, Justin Johnson, Kenji Hata, Joshua Kravitz, Stephanie Chen, Yannis Kalantidis, Li-Jia Li, David A Shamma, et al. Visual genome: Connecting language and vision using crowdsourced dense image annotations. *International journal of computer vision*, 123:32–73, 2017.

Hsin-Ying Lee, Hung-Yu Tseng, and Ming-Hsuan Yang. Exploiting diffusion prior for generalizable dense prediction. In *Proceedings of the IEEE/CVF Conference on Computer Vision and Pattern Recognition*, pp. 7861–7871, 2024.

Boyi Li, Wenqi Ren, Dengpan Fu, Dacheng Tao, Dan Feng, Wenjun Zeng, and Zhangyang Wang. Benchmarking single-image dehazing and beyond. *IEEE Transactions on Image Processing*, 28 (1):492–505, 2018.

Boyun Li, Xiao Liu, Peng Hu, Zhongqin Wu, Jiancheng Lv, and Xi Peng. All-in-one image restoration for unknown corruption. In *Proceedings of the IEEE/CVF conference on computer vision and pattern recognition*, pp. 17452–17462, 2022.

Chongyi Li, Chunle Guo, Wenqi Ren, Runmin Cong, Junhui Hou, Sam Kwong, and Dacheng Tao. An underwater image enhancement benchmark dataset and beyond. *IEEE transactions on image processing*, 29:4376–4389, 2019a.

Feng Li, Hao Zhang, Huaizhe Xu, Shilong Liu, Lei Zhang, Lionel M Ni, and Heung-Yeung Shum. Mask dino: Towards a unified transformer-based framework for object detection and segmentation. In *Proceedings of the IEEE/CVF Conference on Computer Vision and Pattern Recognition*, pp. 3041–3050, 2023.

Ming Li, Taojiannan Yang, Huafeng Kuang, Jie Wu, Zhaoning Wang, Xuefeng Xiao, and Chen Chen. Controlnet++: Improving conditional controls with efficient consistency feedback. *arXiv preprint arXiv:2404.07987*, 2024.

Ruoteng Li, Loong-Fah Cheong, and Robby T Tan. Heavy rain image restoration: Integrating physics model and conditional adversarial learning. In *Proceedings of the IEEE/CVF conference on computer vision and pattern recognition*, pp. 1633–1642, 2019b.

Jingyun Liang, Jiezhang Cao, Guolei Sun, Kai Zhang, Luc Van Gool, and Radu Timofte. Swinir: Image restoration using swin transformer. In *Proceedings of the IEEE/CVF international conference on computer vision*, pp. 1833–1844, 2021.

Tsung-Yi Lin, Michael Maire, Serge Belongie, James Hays, Pietro Perona, Deva Ramanan, Piotr Dollár, and C Lawrence Zitnick. Microsoft coco: Common objects in context. In *Computer Vision–ECCV 2014: 13th European Conference, Zurich, Switzerland, September 6-12, 2014, Proceedings, Part V 13*, pp. 740–755. Springer, 2014.

Yaron Lipman, Ricky T. Q. Chen, Heli Ben-Hamu, Maximilian Nickel, and Matthew Le. Flow matching for generative modeling. In *The Eleventh International Conference on Learning Representations*, 2023. URL https://openreview.net/forum?id=PqvMRDCJT9t.

Chang Liu, Henghui Ding, and Xudong Jiang. Gres: Generalized referring expression segmentation. In *Proceedings of the IEEE/CVF conference on computer vision and pattern recognition*, pp. 23592–23601, 2023a.

Xingchao Liu, Chengyue Gong, and qiang liu. Flow straight and fast: Learning to generate and transfer data with rectified flow. In *The Eleventh International Conference on Learning Representations*, 2023b. URL https://openreview.net/forum?id=XVjTT1nw5z.

Yang Liu, Zhen Zhu, and Xiang Bai. Wdnet: Watermark-decomposition network for visible watermark removal. In *Proceedings of the IEEE/CVF winter conference on applications of computer vision*, pp. 3685–3693, 2021.

Yun-Fu Liu, Da-Wei Jaw, Shih-Chia Huang, and Jenq-Neng Hwang. Desnownet: Context-aware deep network for snow removal. *IEEE Transactions on Image Processing*, 27(6):3064–3073, 2018.

Ziwei Liu, Ping Luo, Xiaogang Wang, and Xiaoou Tang. Deep learning face attributes in the wild. In *Proceedings of International Conference on Computer Vision (ICCV)*, December 2015.

Jiasen Lu, Christopher Clark, Rowan Zellers, Roozbeh Mottaghi, and Aniruddha Kembhavi. Unified-io: A unified model for vision, language, and multi-modal tasks. In *The Eleventh International Conference on Learning Representations*, 2022a.

Jiasen Lu, Christopher Clark, Rowan Zellers, Roozbeh Mottaghi, and Aniruddha Kembhavi. Unified-io: A unified model for vision, language, and multi-modal tasks. In *The Eleventh International Conference on Learning Representations*, 2022b.

Jiasen Lu, Christopher Clark, Sangho Lee, Zichen Zhang, Savya Khosla, Ryan Marten, Derek Hoiem, and Aniruddha Kembhavi. Unified-io 2: Scaling autoregressive multimodal models with vision language audio and action. In *Proceedings of the IEEE/CVF Conference on Computer Vision and Pattern Recognition*, pp. 26439–26455, 2024.

Ziwei Luo, Fredrik K Gustafsson, Zheng Zhao, Jens Sjölund, and Thomas B Schön. Controlling vision-language models for universal image restoration. *arXiv preprint arXiv:2310.01018*, 2023.

Nanye Ma, Mark Goldstein, Michael S Albergo, Nicholas M Boffi, Eric Vanden-Eijnden, and Saining Xie. Sit: Exploring flow and diffusion-based generative models with scalable interpolant transformers. *arXiv preprint arXiv:2401.08740*, 2024.

David Martin, Charless Fowlkes, Doron Tal, and Jitendra Malik. A database of human segmented natural images and its application to evaluating segmentation algorithms and measuring ecological statistics. In *Proceedings eighth IEEE international conference on computer vision. ICCV 2001*, volume 2, pp. 416–423. IEEE, 2001.

David Mizrahi, Roman Bachmann, Oguzhan Kar, Teresa Yeo, Mingfei Gao, Afshin Dehghan, and Amir Zamir. 4m: Massively multimodal masked modeling. *Advances in Neural Information Processing Systems*, 36, 2024.

Chong Mou, Xintao Wang, Liangbin Xie, Yanze Wu, Jian Zhang, Zhongang Qi, and Ying Shan. T2i-adapter: Learning adapters to dig out more controllable ability for text-to-image diffusion models. In *Proceedings of the AAAI Conference on Artificial Intelligence*, volume 38, pp. 4296–4304, 2024.

Seungjun Nah, Tae Hyun Kim, and Kyoung Mu Lee. Deep multi-scale convolutional neural network for dynamic scene deblurring. In *Proceedings of the IEEE conference on computer vision and pattern recognition*, pp. 3883–3891, 2017.

Seungjun Nah, Sungyong Baik, Seokil Hong, Gyeongsik Moon, Sanghyun Son, Radu Timofte, and Kyoung Mu Lee. Ntire 2019 challenge on video deblurring and super-resolution: Dataset and study. In *CVPR Workshops*, June 2019.

William Peebles and Saining Xie. Scalable diffusion models with transformers. In *Proceedings of the IEEE/CVF International Conference on Computer Vision*, pp. 4195–4205, 2023.

Bowen Peng and Jeffrey Quesnelle. Ntk-aware scaled rope allows llama models to have extended (8k+) context size without any fine-tuning and minimal perplexity degradation, 2023.

Dustin Podell, Zion English, Kyle Lacey, Andreas Blattmann, Tim Dockhorn, Jonas Müller, Joe Penna, and Robin Rombach. Sdxl: Improving latent diffusion models for high-resolution image synthesis. *arXiv preprint arXiv:2307.01952*, 2023.

Vaishnav Potlapalli, Syed Waqas Zamir, Salman H Khan, and Fahad Shahbaz Khan. Promptir: Prompting for all-in-one image restoration. *Advances in Neural Information Processing Systems*, 36, 2024.

Rui Qian, Robby T Tan, Wenhan Yang, Jiajun Su, and Jiaying Liu. Attentive generative adversarial network for raindrop removal from a single image. In *Proceedings of the IEEE conference on computer vision and pattern recognition*, pp. 2482–2491, 2018.

Liangqiong Qu, Jiandong Tian, Shengfeng He, Yandong Tang, and Rynson WH Lau. Deshadownet: A multi-context embedding deep network for shadow removal. In *Proceedings of the IEEE conference on computer vision and pattern recognition*, pp. 4067–4075, 2017.

Ruijie Quan, Xin Yu, Yuanzhi Liang, and Yi Yang. Removing raindrops and rain streaks in one go. In *Proceedings of the IEEE/CVF conference on computer vision and pattern recognition*, pp. 9147–9156, 2021.

Alec Radford, Jong Wook Kim, Chris Hallacy, Aditya Ramesh, Gabriel Goh, Sandhini Agarwal, Girish Sastry, Amanda Askell, Pamela Mishkin, Jack Clark, et al. Learning transferable visual models from natural language supervision. In *International conference on machine learning*, pp. 8748–8763. PMLR, 2021.

Aditya Ramesh, Mikhail Pavlov, Gabriel Goh, Scott Gray, Chelsea Voss, Alec Radford, Mark Chen, and Ilya Sutskever. Zero-shot text-to-image generation. In *International conference on machine learning*, pp. 8821–8831. Pmlr, 2021.

Yongming Rao, Wenliang Zhao, Benlin Liu, Jiwen Lu, Jie Zhou, and Cho-Jui Hsieh. Dynamicvit: Efficient vision transformers with dynamic token sparsification. *Advances in neural information processing systems*, 34:13937–13949, 2021.

Jaesung Rim, Haeyun Lee, Jucheol Won, and Sunghyun Cho. Real-world blur dataset for learning and benchmarking deblurring algorithms. In *Computer Vision–ECCV 2020: 16th European Conference, Glasgow, UK, August 23–28, 2020, Proceedings, Part XXV 16*, pp. 184–201. Springer, 2020.

Mike Roberts, Jason Ramapuram, Anurag Ranjan, Atulit Kumar, Miguel Angel Bautista, Nathan Paczan, Russ Webb, and Joshua M. Susskind. Hypersim: A photorealistic synthetic dataset for holistic indoor scene understanding. In *International Conference on Computer Vision (ICCV) 2021*, 2021.

Robin Rombach, Andreas Blattmann, Dominik Lorenz, Patrick Esser, and Björn Ommer. High-resolution image synthesis with latent diffusion models. In *Proceedings of the IEEE/CVF conference on computer vision and pattern recognition*, pp. 10684–10695, 2022a.

Robin Rombach, Andreas Blattmann, Dominik Lorenz, Patrick Esser, and Björn Ommer. High-resolution image synthesis with latent diffusion models. In *Proceedings of the IEEE/CVF conference on computer vision and pattern recognition*, pp. 10684–10695, 2022b.

Chitwan Saharia, William Chan, Huiwen Chang, Chris Lee, Jonathan Ho, Tim Salimans, David Fleet, and Mohammad Norouzi. Palette: Image-to-image diffusion models. In *ACM SIGGRAPH 2022 conference proceedings*, pp. 1–10, 2022a.

Chitwan Saharia, William Chan, Saurabh Saxena, Lala Li, Jay Whang, Emily L Denton, Kamyar Ghasemipour, Raphael Gontijo Lopes, Burcu Karagol Ayan, Tim Salimans, et al. Photorealistic text-to-image diffusion models with deep language understanding. *Advances in neural information processing systems*, 35:36479–36494, 2022b.

Chitwan Saharia, Jonathan Ho, William Chan, Tim Salimans, David J Fleet, and Mohammad Norouzi. Image super-resolution via iterative refinement. *IEEE transactions on pattern analysis and machine intelligence*, 45(4):4713–4726, 2022c.

Christoph Schuhmann, Romain Beaumont, Richard Vencu, Cade Gordon, Ross Wightman, Mehdi Cherti, Theo Coombes, Aarush Katta, Clayton Mullis, Mitchell Wortsman, et al. Laion-5b: An open large-scale dataset for training next generation image-text models. *Advances in Neural Information Processing Systems*, 35:25278–25294, 2022.

Shelly Sheynin, Adam Polyak, Uriel Singer, Yuval Kirstain, Amit Zohar, Oron Ashual, Devi Parikh, and Yaniv Taigman. Emu edit: Precise image editing via recognition and generation tasks. In *Proceedings of the IEEE/CVF Conference on Computer Vision and Pattern Recognition*, pp. 8871–8879, 2024.

Jing Shi, Ning Xu, Trung Bui, Franck Dernoncourt, Zheng Wen, and Chenliang Xu. A benchmark and baseline for language-driven image editing. In *Proceedings of the Asian Conference on Computer Vision*, 2020.

Nathan Silberman, Derek Hoiem, Pushmeet Kohli, and Rob Fergus. Indoor segmentation and support inference from rgbd images. In *Computer Vision–ECCV 2012: 12th European Conference on Computer Vision, Florence, Italy, October 7-13, 2012, Proceedings, Part V 12*, pp. 746–760. Springer, 2012.

Jascha Sohl-Dickstein, Eric Weiss, Niru Maheswaranathan, and Surya Ganguli. Deep unsupervised learning using nonequilibrium thermodynamics. In *International conference on machine learning*, pp. 2256–2265. PMLR, 2015.

Yang Song and Stefano Ermon. Generative modeling by estimating gradients of the data distribution. *Advances in neural information processing systems*, 32, 2019.

Yang Song, Jascha Sohl-Dickstein, Diederik P Kingma, Abhishek Kumar, Stefano Ermon, and Ben Poole. Score-based generative modeling through stochastic differential equations. In *International Conference on Learning Representations*, 2021. URL https://openreview.net/forum?id=PxTIG12RRHS.

Xavier Soria, Yachuan Li, Mohammad Rouhani, and Angel D. Sappa. Tiny and efficient model for the edge detection generalization. In *Proceedings of the IEEE/CVF International Conference on Computer Vision (ICCV) Workshops*, pp. 1364–1373, October 2023.

Jianlin Su, Murtadha Ahmed, Yu Lu, Shengfeng Pan, Wen Bo, and Yunfeng Liu. Roformer: Enhanced transformer with rotary position embedding. *Neurocomputing*, 568:127063, 2024.

Quan Sun, Qiying Yu, Yufeng Cui, Fan Zhang, Xiaosong Zhang, Yueze Wang, Hongcheng Gao, Jingjing Liu, Tiejun Huang, and Xinlong Wang. Emu: Generative pretraining in multimodality. In *The Twelfth International Conference on Learning Representations*, 2023.

Roman Suvorov, Elizaveta Logacheva, Anton Mashikhin, Anastasia Remizova, Arsenii Ashukha, Aleksei Silvestrov, Naejin Kong, Harshith Goka, Kiwoong Park, and Victor Lempitsky. Resolution-robust large mask inpainting with fourier convolutions. In *Proceedings of the IEEE/CVF winter conference on applications of computer vision*, pp. 2149–2159, 2022.

Gemma Team, Thomas Mesnard, Cassidy Hardin, Robert Dadashi, Surya Bhupatiraju, Shreya Pathak, Laurent Sifre, Morgane Rivière, Mihir Sanjay Kale, Juliette Love, et al. Gemma: Open models based on gemini research and technology. *arXiv preprint arXiv:2403.08295*, 2024.

Guy Tevet, Sigal Raab, Brian Gordon, Yoni Shafir, Daniel Cohen-or, and Amit Haim Bermano. Human motion diffusion model. In *The Eleventh International Conference on Learning Representations*, 2023. URL https://openreview.net/forum?id=SJ1kSyO2jwu.

Alexander Tong, Kilian FATRAS, Nikolay Malkin, Guillaume Huguet, Yanlei Zhang, Jarrid Rector-Brooks, Guy Wolf, and Yoshua Bengio. Improving and generalizing flow-based generative models with minibatch optimal transport. *Transactions on Machine Learning Research*, 2024. ISSN 2835-8856. URL https://openreview.net/forum?id=CD9Snc73AW. Expert Certification.

Hugo Touvron, Thibaut Lavril, Gautier Izacard, Xavier Martinet, Marie-Anne Lachaux, Timothée Lacroix, Baptiste Rozière, Naman Goyal, Eric Hambro, Faisal Azhar, et al. Llama: Open and efficient foundation language models. *arXiv preprint arXiv:2302.13971*, 2023.

Aaron Van Den Oord, Oriol Vinyals, et al. Neural discrete representation learning. *Advances in neural information processing systems*, 30, 2017.

Ashish Vaswani, Noam Shazeer, Niki Parmar, Jakob Uszkoreit, Llion Jones, Aidan N Gomez, Łukasz Kaiser, and Illia Polosukhin. Attention is all you need. *Advances in neural information processing systems*, 30, 2017.

Longguang Wang, Yulan Guo, Yingqian Wang, Juncheng Li, Shuhang Gu, Radu Timofte, Ming Cheng, Haoyu Ma, Qiufang Ma, Xiaopeng Sun, et al. Ntire 2023 challenge on stereo image super-resolution: Methods and results. In *Proceedings of the IEEE/CVF conference on computer vision and pattern recognition*, pp. 1346–1372, 2023a.

Peng Wang, An Yang, Rui Men, Junyang Lin, Shuai Bai, Zhikang Li, Jianxin Ma, Chang Zhou, Jingren Zhou, and Hongxia Yang. Ofa: Unifying architectures, tasks, and modalities through a simple sequence-to-sequence learning framework. In *International conference on machine learning*, pp. 23318–23340. PMLR, 2022a.

Tengfei Wang, Ting Zhang, Bo Zhang, Hao Ouyang, Dong Chen, Qifeng Chen, and Fang Wen. Pretraining is all you need for image-to-image translation. *arXiv preprint arXiv:2205.12952*, 2022b.

Xinlong Wang, Wen Wang, Yue Cao, Chunhua Shen, and Tiejun Huang. Images speak in images: A generalist painter for in-context visual learning. In *Proceedings of the IEEE/CVF Conference on Computer Vision and Pattern Recognition*, pp. 6830–6839, 2023b.

Zhaoqing Wang, Yu Lu, Qiang Li, Xunqiang Tao, Yandong Guo, Mingming Gong, and Tongliang Liu. Cris: Clip-driven referring image segmentation. In *Proceedings of the IEEE/CVF conference on computer vision and pattern recognition*, pp. 11686–11695, 2022c.

Zhendong Wang, Yifan Jiang, Yadong Lu, Pengcheng He, Weizhu Chen, Zhangyang Wang, Mingyuan Zhou, et al. In-context learning unlocked for diffusion models. *Advances in Neural Information Processing Systems*, 36:8542–8562, 2023c.

Shengqiong Wu, Hao Fei, Leigang Qu, Wei Ji, and Tat-Seng Chua. Next-gpt: Any-to-any multimodal llm. In *Forty-first International Conference on Machine Learning*.

Xiaoshi Wu, Yiming Hao, Keqiang Sun, Yixiong Chen, Feng Zhu, Rui Zhao, and Hongsheng Li. Human preference score v2: A solid benchmark for evaluating human preferences of text-to-image synthesis. *arXiv preprint arXiv:2306.09341*, 2023.

Bin Xia, Yulun Zhang, Shiyin Wang, Yitong Wang, Xinglong Wu, Yapeng Tian, Wenming Yang, and Luc Van Gool. Diffir: Efficient diffusion model for image restoration. In *Proceedings of the IEEE/CVF International Conference on Computer Vision*, pp. 13095–13105, 2023.

Xiaoyu Xiang, Ding Liu, Xiao Yang, Yiheng Zhu, and Xiaohui Shen. Anime2sketch: A sketch extractor for anime arts with deep networks, 2021. https://github.com/mukosame/anime2sketch.

Saining Xie and Zhuowen Tu. Holistically-nested edge detection. In *IEEE International Conference on Computer Vision*, 2015.

Jiarui Xu, Sifei Liu, Arash Vahdat, Wonmin Byeon, Xiaolong Wang, and Shalini De Mello. Open-vocabulary panoptic segmentation with text-to-image diffusion models. In *Proceedings of the IEEE/CVF Conference on Computer Vision and Pattern Recognition*, pp. 2955–2966, 2023.

Lihe Yang, Bingyi Kang, Zilong Huang, Xiaogang Xu, Jiashi Feng, and Hengshuang Zhao. Depth anything: Unleashing the power of large-scale unlabeled data. In *Proceedings of the IEEE/CVF Conference on Computer Vision and Pattern Recognition*, pp. 10371–10381, 2024a.

Lihe Yang, Bingyi Kang, Zilong Huang, Zhen Zhao, Xiaogang Xu, Jiashi Feng, and Hengshuang Zhao. Depth anything v2. *arXiv:2406.09414*, 2024b.

Wenhan Yang, Robby T Tan, Jiashi Feng, Jiaying Liu, Zongming Guo, and Shuicheng Yan. Deep joint rain detection and removal from a single image. In *Proceedings of the IEEE conference on computer vision and pattern recognition*, pp. 1357–1366, 2017.

Wenhan Yang, Wenjing Wang, Haofeng Huang, Shiqi Wang, and Jiaying Liu. Sparse gradient regularized deep retinex network for robust low-light image enhancement. *IEEE Transactions on Image Processing*, 30:2072–2086, 2021.

Zhao Yang, Jiaqi Wang, Yansong Tang, Kai Chen, Hengshuang Zhao, and Philip HS Torr. Lavt: Language-aware vision transformer for referring image segmentation. In *Proceedings of the IEEE/CVF Conference on Computer Vision and Pattern Recognition*, pp. 18155–18165, 2022.

Yuan Yao, Tianyu Yu, Ao Zhang, Chongyi Wang, Junbo Cui, Hongji Zhu, Tianchi Cai, Haoyu Li, Weilin Zhao, Zhihui He, et al. Minicpm-v: A gpt-4v level mllm on your phone. *arXiv preprint arXiv:2408.01800*, 2024.

Hanrong Ye and Dan Xu. Inverted pyramid multi-task transformer for dense scene understanding. In *European Conference on Computer Vision*, pp. 514–530. Springer, 2022.

Hu Ye, Jun Zhang, Sibo Liu, Xiao Han, and Wei Yang. Ip-adapter: Text compatible image prompt adapter for text-to-image diffusion models. *arXiv preprint arXiv:2308.06721*, 2023.

Ahmet Burak Yildirim, Vedat Baday, Erkut Erdem, Aykut Erdem, and Aysegul Dundar. Inst-inpaint: Instructing to remove objects with diffusion models. *arXiv preprint arXiv:2304.03246*, 2023.

Jiahui Yu, Zhe Lin, Jimei Yang, Xiaohui Shen, Xin Lu, and Thomas S Huang. Free-form image inpainting with gated convolution. In *Proceedings of the IEEE/CVF international conference on computer vision*, pp. 4471–4480, 2019.

Licheng Yu, Patrick Poirson, Shan Yang, Alexander C Berg, and Tamara L Berg. Modeling context in referring expressions. In *Computer Vision–ECCV 2016: 14th European Conference, Amsterdam, The Netherlands, October 11-14, 2016, Proceedings, Part II 14*, pp. 69–85. Springer, 2016.

Xin Yu, Peng Dai, Wenbo Li, Lan Ma, Jiajun Shen, Jia Li, and Xiaojuan Qi. Towards efficient and scale-robust ultra-high-definition image demoiréing. In *European Conference on Computer Vision*, pp. 646–662. Springer, 2022.

Syed Waqas Zamir, Aditya Arora, Salman Khan, Munawar Hayat, Fahad Shahbaz Khan, and Ming-Hsuan Yang. Restormer: Efficient transformer for high-resolution image restoration. In *Proceedings of the IEEE/CVF conference on computer vision and pattern recognition*, pp. 5728–5739, 2022.

Kai Zhang, Lingbo Mo, Wenhu Chen, Huan Sun, and Yu Su. Magicbrush: A manually annotated dataset for instruction-guided image editing. *Advances in Neural Information Processing Systems*, 36, 2024a.

Lvmin Zhang, Anyi Rao, and Maneesh Agrawala. Adding conditional control to text-to-image diffusion models. In *Proceedings of the IEEE/CVF International Conference on Computer Vision*, pp. 3836–3847, 2023a.

Mingyuan Zhang, Zhongang Cai, Liang Pan, Fangzhou Hong, Xinying Guo, Lei Yang, and Ziwei Liu. Motiondiffuse: Text-driven human motion generation with diffusion model. *IEEE Transactions on Pattern Analysis and Machine Intelligence*, 2024b.

Renrui Zhang, Zhengkai Jiang, Ziyu Guo, Shilin Yan, Junting Pan, Hao Dong, Peng Gao, and Hongsheng Li. Personalize segment anything model with one shot. *ICLR 2024*, 2023b.

Renrui Zhang, Jiaming Han, Chris Liu, Aojun Zhou, Pan Lu, Yu Qiao, Hongsheng Li, and Peng Gao. Llama-adapter: Efficient fine-tuning of large language models with zero-initialized attention. In *ICLR 2024*, 2024c.

Renrui Zhang, Dongzhi Jiang, Yichi Zhang, Haokun Lin, Ziyu Guo, Pengshuo Qiu, Aojun Zhou, Pan Lu, Kai-Wei Chang, Peng Gao, et al. Mathverse: Does your multi-modal llm truly see the diagrams in visual math problems? *ECCV 2024*, 2024d.

Renrui Zhang, Xinyu Wei, Dongzhi Jiang, Yichi Zhang, Ziyu Guo, Chengzhuo Tong, Jiaming Liu, Aojun Zhou, Bin Wei, Shanghang Zhang, et al. Mavis: Mathematical visual instruction tuning. *arXiv preprint arXiv:2407.08739*, 2024e.

Shiwen Zhang, Shuai Xiao, and Weilin Huang. Forgedit: Text guided image editing via learning and forgetting. *arXiv preprint arXiv:2309.10556*, 2023c.

Haozhe Zhao, Xiaojian Ma, Liang Chen, Shuzheng Si, Rujie Wu, Kaikai An, Peiyu Yu, Minjia Zhang, Qing Li, and Baobao Chang. Ultraedit: Instruction-based fine-grained image editing at scale. *arXiv preprint arXiv:2407.05282*, 2024.

Bolei Zhou, Agata Lapedriza, Jianxiong Xiao, Antonio Torralba, and Aude Oliva. Learning deep features for scene recognition using places database. *Advances in neural information processing systems*, 27, 2014.

Bolei Zhou, Agata Lapedriza, Aditya Khosla, Aude Oliva, and Antonio Torralba. Places: A 10 million image database for scene recognition. *IEEE transactions on pattern analysis and machine intelligence*, 40(6):1452–1464, 2017a.

Bolei Zhou, Hang Zhao, Xavier Puig, Sanja Fidler, Adela Barriuso, and Antonio Torralba. Scene parsing through ade20k dataset. In *Proceedings of the IEEE conference on computer vision and pattern recognition*, pp. 633–641, 2017b.

Yuqian Zhou, David Ren, Neil Emerton, Sehoon Lim, and Timothy Large. Image restoration for under-display camera. In *Proceedings of the ieee/cvf conference on computer vision and pattern recognition*, pp. 9179–9188, 2021.

Yurui Zhu, Tianyu Wang, Xueyang Fu, Xuanyu Yang, Xin Guo, Jifeng Dai, Yu Qiao, and Xiaowei Hu. Learning weather-general and weather-specific features for image restoration under multiple adverse weather conditions. In *Proceedings of the IEEE/CVF conference on computer vision and pattern recognition*, pp. 21747–21758, 2023.

Le Zhuo, Ruoyi Du, Han Xiao, Yangguang Li, Dongyang Liu, Rongjie Huang, Wenze Liu, Lirui Zhao, Fu-Yun Wang, Zhanyu Ma, et al. Lumina-next: Making lumina-t2x stronger and faster with next-dit. *arXiv preprint arXiv:2406.18583*, 2024.

APPENDIX

A RELATED WORK

Diffusion Models. Diffusion models estimate the data distribution by modeling the gradient of the noise-perturbed data distributions (Sohl-Dickstein et al., 2015; Song & Ermon, 2019; Ho et al., 2020; Dhariwal & Nichol, 2021; Song et al., 2021). They have demonstrated remarkable performance in various fields, ranging from text-to-image generation (Rombach et al., 2022a; Saharia et al., 2022b; Betker et al., 2023; Jiang et al., 2024a; Zhang et al., 2023b), controllable generation (Zhang et al., 2023a; Ye et al., 2023), and image editing (Avrahami et al., 2022; Brooks et al., 2023; Kawar et al., 2023) to video (Ho et al., 2022; Brooks et al., 2024), audio (Kong et al., 2021; Huang et al., 2023), 3D (Guo et al., 2023; 2024), and motion (Tevet et al., 2023; Zhang et al., 2024b) generation. Beyond generation, recent works have also exhibited diffusion models' capabilities in computer vision tasks, such as semantic segmentation (Baranchuk et al., 2022; Xu et al., 2023), depth estimation (Ke et al., 2024b; Lee et al., 2024), and image restoration (Xia et al., 2023). Benefiting from the visual knowledge learned from large-scale pretraining, these works open up the potential for adapting pretrained diffusion models to downstream tasks in a generative manner, with excellent capabilities like handling inherent uncertainties and zero-shot generalization.

Vision Generalists. Building a vision generalist capable of unifying various visual tasks has been a long-standing goal. Inspired by the success of scaling sequential modeling with transformers in natural language processing, many vision generalists (Wang et al., 2022a; Chen et al., 2022b; Lu et al., 2022b; 2024; Mizrahi et al., 2024; Bachmann et al., 2024; Bai et al., 2024) follow a similar approach by converting inputs and outputs into sequences of discrete tokens (Van Den Oord et al., 2017; Esser et al., 2021), allowing joint modeling of different modalities within a unified framework. With the rapid advancements in large language models (LLMs) (Achiam et al., 2023; Touvron et al., 2023; Zhang et al., 2024c) and multi-modal large language models (MLLMs) (Gao et al., 2024; Zhang et al., 2024e;d; Jiang et al., 2024b), several works (Koh et al., 2024; Dong et al., 2024; Sun et al., 2023; Wu et al.; Han et al., 2023) have introduced task-specific tokens, aligning them with the embedding space of LLMs to equip text-only LLMs with the ability to perceive and generate images. However, a common drawback of these approaches is their limited performance on generation tasks, such as text-to-image generation and image editing. Additionally, their sampling efficiency is constrained by the next-token prediction paradigm, which worsens for image-to-image tasks or when working with high-resolution images. In contrast, diffusion models, known for their state-of-the-art generation performance and efficiency, are ideal candidates for image generation and manipulation tasks. Recent efforts (Wang et al., 2023c; Gan et al., 2024; Hu et al., 2024; Geng et al., 2024) aim to create a visual generalist by unifying multiple visual tasks through a natural language interface based on pretrained text-to-image diffusion. However, these models generally focus on a limited set of tasks within narrow domains and are constrained by the scalability limitations of early foundation models (Rombach et al., 2022b), limiting their potential as practical visual assistants. To address these challenges, we propose a solution from both the model and data perspectives to develop a more versatile visual assistant.

B MORE DETAILS FOR THE OMNI PEXEL-TO-PEXEL INSTRUCTION-TUNING DATASET

B.1 IMAGE RESTORATION

All the open-source datasets used for the image restoration task are listed below.

BSD (2001)	RealBlur (2020)	DPDD (2020)	GoPro (2017)	REDS (2019)
DenseHaze (2019)	NH-HAZE (2020)	Reside-6K (2018)	UHDM (2022)	SIDD (2018)
Rain1400 (2017)	Outdoor-Rain (2019b)	SSID (2022)	RainDrop (2018)	RainDS (2021)
SRD (2017)	RealSnow (2023)	Snow100K (2018)	CLWD (2021)	CelebA-HQ (2015)
RealSR (2019)	LOL-v2 (2021)	DIV2K (2017)	FFHQ (2019)	Flickr2K (2023a)

B.2 IMAGE GROUNDING

(1) Segmentation Referring. We define referring segmentation as highlighting the target object specified by the user in the output image. For example, if the model is given instructions like, "Please mark the pixels in {color} based on the referring description: {caption}," the resulting image would display a mask in the specified color over the appropriate object described in the caption. When constructing the data, we pre-set the mask to a specific color with 50% opacity and apply it directly to the original image. This method makes it easier for humans to evaluate the accuracy of the predicted mask.

(2) Box Detection Referring. Instead of pixel-level grounding, we use bounding boxes to highlight the target object specified by the user in the output image. Prompts for this task include instructions like, "Mark the specified area with a bounding box in {color}: {caption}." The model then frames the described object with a bounding box in the specified color. Similar to referring segmentation, we pre-set the bounding box to a specific color and apply it directly to the original image to produce the final output. During inference, we follow the post-processing methods outlined in InstructCV (Sec. A.3) (Gan et al., 2024) to derive the coordinates of the specified region from the output image.

(3) Binary Mask Prediction. To promote the use of referring segmentation in real-world scenarios, we shift the objective from rendering images to directly predicting a binary mask. The prompt for this task might be: "Generate a binary mask for the described object: {caption}." The model is expected to produce a binary mask image where the object described in the caption is represented as a white region, with the background in black, excluding any original image content. Since the binary mask is a single-channel image, we replicate the mask across three channels to convert it into RGB space during training.

B.3 CONTROLLABLE GENERATION

Canny Edge to Image. We use a Canny edge detector (Canny, 1986) (with random thresholds) and a Tiny and Efficient Edge Detector (TEED) (Soria et al., 2023) to obtain 1M canny-image-caption pairs from our collected natural images.

Holistically-Nested Edge(HED) Boundary to Image. We use HED boundary detection (Xie & Tu, 2015) to obtain 1M edge-image-caption pairs from our collected natural images (a part of images are source of the Canny Edge dataset.)

Depth Map to Image. Depth information is crucial for producing images with a sense of three-dimensionality. We used the Depth Anything V2 model (Yang et al., 2024b) obtain 1M depth-image-caption pairs, enabling accurate generation of depth maps across different visual scenarios.

User Sketch to Image. Following ControlNet (Zhang et al., 2023a), we generate human sketches from images by applying HED boundary detection (Xie & Tu, 2015) combined with strong data augmentations, including random thresholds, random masking of sketch portions, random morphological transformations, and random non-maximum suppression. This process results in 0.4 million sketch-image-caption pairs.

Human Pose to Image. For human pose-based generation, we employed the OpenPose model (Cao et al., 2017) for real-time multi-person 2D pose estimation. To ensure quality, only images where at least 30% of the key points of the whole body were detected were retained; those with fewer detected key points were discarded. We directly use visualized pose images with human skeletons as input condition. Finally, we obtain 0.25M pose-image-caption pairs.

Semantic Segmentation to Image. The semantic mask annotation is produced using OneFormer (Jain et al., 2023), as adopted in ControlNet-1.1 [1], providing precise segmentation maps as conditions for image generation. This process results in 1M seg-image-caption pairs.

Normal Map to Image. The surface normals are generated using DSINE (Bae & Davison, 2024), which contributed to the depiction of surface orientation and texture details in the generated images. Finally, we obtain 0.8M normal-image-caption pairs.

[1] https://github.com/lllyasviel/ControlNet-v1-1-nightly

Line-art to Image. We use a cartoon line drawing extraction method (Xiang et al., 2021) to generate line drawings from cartoons. This process yields 0.8M normal-image-caption pairs.

B.4 Dense Image Prediction

Depth Estimation. Monocular depth estimation is a dense prediction task to estimate the per-pixel depth value(distance relative to the camera) given an input RGB image. The datasets we use include Hypersim (Roberts et al., 2021) and VKITTI 2 (Cabon et al., 2020), and our collected depth maps from controllable dataset. For different datasets, the ground-truth depth for each pixel may vary, being either an absolute depth value or a relative depth value. Here we uniformly map the ground-truth value from real-valued range to the integer RGB space with range $[0, 255]$, and let the three channels be the same ground truth. During inference, we directly average the outputs of the three channels, and then perform an inverse linear transformation specific to each dataset to obtain a depth estimate in the real-valued range.

Surface Normal Estimation. For surface normal estimation, we train the model to generate RGB images that encode pixel orientations differently. We convert the $x/y/z$ orientations into $r/g/b$ values to create a normal map visualization. The datasets we use include NYUv2 (Silberman et al., 2012) and our collected surface normals maps from controllable dataset.

Semantic Segmentation. Semantic segmentation is a dense prediction task to predict the per-pixel semantic label given an input image. Given a semantic segmentation task, we formulate different semantic categories using different colors in RGB space. Specifically, we define the background and ignore areas as black, i.e., pixels in color $(0, 0, 0)$, and generate the colors for foreground categories using the pre-defined color-label dictionary. During inference, to decode the output image to a single channel map where each pixel represents a class label, we compute the L2 distance between each output pixel and the pre-defined colors for each semantic category, and take the label of the closest color as the predicted category. The datasets we use is ADE20K (Zhou et al., 2017b), which covers a broad range of 150 semantic categories.

B.5 Instruction Prompt Examples.

Handling free-form user prompts, rather than relying on fixed task-specific prompts, significantly enhances PixWizard's flexibility and usability as a general visual assistant. In Fig. 10, we showcase various examples where task-specific templates are dynamically rephrased and adapted by GPT-4o

C More Details for the Architecture

C.1 Preliminaries

Diffusion Transformers. Diffusion models (Sohl-Dickstein et al., 2015; Ho et al., 2020; Dhariwal & Nichol, 2021; Song et al., 2021) are a family of generative models demonstrating remarkable performance in modeling data distributions. These models are trained to estimate clean data samples (or added noise) from their noisy version perturbed by a pre-defined Gaussian noise schedule. During sampling, they can generate data samples by iterative denoising starting from prior Gaussian distributions. Recent advancements in diffusion models, such as SoRA (Brooks et al., 2024), SD3 (Esser et al., 2024), and PixArt (Chen et al., 2024b;a), exhibiting a paradigm shift from the classic diffusion U-Net architecture to diffusion transformers (DiTs) (Peebles & Xie, 2023). DiTs appear to be a unified architecture with minimal modifications to original transformers (Vaswani et al., 2017). Therefore, these models demonstrate better scaling properties and can be naturally extended to more modalities, such as integrating text and image conditions through cross-attention.

Flow-based Models. Another line of generative models that extends the definition of diffusion models is ODE-based continuous normalizing flows (Chen et al., 2018), which are also known as flow matching (Lipman et al., 2023; Tong et al., 2024; Albergo & Vanden-Eijnden, 2023) or rectified flows (Liu et al., 2023b). Specifically, given the data space $\mathbb{R}^d$ with samples $x \in \mathbb{R}^d$, flow-based models aim to learn a time-dependent velocity field $v : [0, 1] \times \mathbb{R}^d \to \mathbb{R}^d$ leading to a flow $\phi : [0, 1] \times \mathbb{R}^d \to \mathbb{R}^d$ that can push noise $x_0 \sim p_0(x_0)$ from source distribution to data $x_1 \sim p_1(x_1)$ from target distribution. This velocity field and associated flow can be defined by an ordinary

Denoise
- Remove the noise and grain from this image.
- Make this photo clearer by getting rid of the noise.
- Reduce the noise and grain in this picture.

...

Dehaze
- Fix the haze in this picture.
- Clear the haze to reveal the details in this picture.
- Remove the mist from this picture.

...

Derain
- Take away the rain.
- Get rid of the rain patterns to show the details better.
- Make this photo clearer by filtering out the raindrops.

...

Deblur
- Make this unclear photo sharper.
- Fix the blurriness in this image.
- Rectify the vagueness of this blurred image.

...

Demoire
- Eliminate the Moiré patterns in this image.
- Reduce the ripple-like distortion in this photo.
- Smooth out the textured distortion in this picture.

...

Demoire
- Eliminate the Moiré patterns in this image.
- Reduce the ripple-like distortion in this photo.
- Smooth out the textured distortion in this picture.

...

Deshadow
- Remove the shadows to make this picture look better.
- Get rid of the dark areas for a clearer image.
- Removing the shadows.

...

Desnow
- Erase the frost to restore visibility in this image.
- Remove the snow to get a clearer view.
- Improve the image by taking out the snow.

...

Dewatermark
- Erase the watermark for a clear view of this photo.
- Get rid of the watermark to fix the visual interference.
- Clean the image by removing any stamps or watermarks.

...

Low-Light Enhancement
- Fix lighting.
- Enhance the visibility in this dimly lit photograph.
- Enhance the image by increasing its brightness and contrast.

...

Flash Remove
- Remove the lens flare and flash reflections.
- Clear the bright glare from the camera flash.
- Get rid of the intrusive light reflections for a cleaner look.

...

Super-Res
- Use super-resolution to make the image sharper and more detailed.
- Improve the resolution to make the image clearer and more detailed.

...

Restoration (Color)
- Restore the original colors in this image.
- Correct the faded colors to reveal the real complexion.
- Improve the color balance for a more accurate view of this ecosystem.

...

Restoration
- Make this image clearer to show its features.
- Fix the blurry image to improve visibility and detail.
- Restore the image.

...

Restoration w/ cap
- Enhance this image for clarity, guided by this description: {caption}.
- Recover the image details using the caption:{caption}
- Eliminate the fuzziness in this picture to make it clear as described: {caption}.

...

Grounding (Box)
- Detect, {color}: {caption}
- Draw a bounding box around the object, using {color}: {caption}
- Use a {color} box to outline the target area: {caption}

...

Grounding (Seg)
- Locate the subject, {color}: {caption}
- Identify and highlight the areas, {color}: {caption}
- Mark the pixels of {caption} in {color} and leave the rest unchanged.

...

Grounding (Mask)
- Extract the binary mask image based on the object description: {caption}
- Create a binary mask representing the object as described in: {caption}
- Grounding, extract the binary mask: {caption}

...

Inpainting
- Complete the image based on the description: {caption}
- Inpainting: {caption}
- Use the caption below to guide the inpainting of the image: {caption}

...

Outpainting
- Outpaint the image with the description: {caption}
- Extend the image, keeping the same style and theme as specified in the description: {caption}

...

Text-to-Image
- Image generation: {caption}
- Produce an image according to the following description: {caption}
- Drawing: {caption}

...

Dense Image Pred.
- Process the image with Canny edge detection and show the edges.
- Generate a depth map that shows the distance of objects in the image.
- Make a HED map that shows the main structures and outlines in the image.
- Generate a human pose map from the image, showing the posture and positions.
- Process the image to show the categorization of the scene's parts.
- Turn this image into a sketch map that outlines the scene's major components.
- Turn this image into a sketch map that outlines the scene's major components.

Controllable Generation
- Turn the Canny edge map into a natural image, inspired by this caption:{caption}
- Create an image based on the depth map and text instructions: {caption}
- HED edge map to image: {caption}
- Generate an image using human pose control: {caption}
- Create a detailed image based on the input's control and text: {caption}
- Condition map to image: {caption}
- Using the provided location to create an image: {caption}

Figure 10: Examples of GPT4o-paraphrase user prompts for different task.

differential equation (ODE): $\frac{d}{dt}\phi_t(x) = v_t(\phi_t(x), t)$ where $\phi_0(x) = x$. Similar to the denoising network in diffusion models, the Flow Matching (FM) objective trains a time-dependent network $v_\theta(x_t, t)$ to regress against the ground truth velocity field $u_t(x_t, t)$. However, direct computation of this FM objective is intractable in practice, since there is no closed-form solution of $u_t(x_t, t)$. Instead, we can minimize the tractable Conditional Flow Matching (CFM) objective defined as:

$$\mathcal{L}_{\text{CFM}}(\theta) = \mathbb{E}_{t, p_1(x_1), p_t(x_t|x_1)} \|v_\theta(x_t, t) - u_t(x_t, t|x_1)\|^2, \tag{7}$$

where $t \sim \mathcal{U}(0, 1)$, $x_1 \sim p_1(x_1)$, and $x_t \sim p_t(x_t|x_1)$. It has been validated that the FM and CFM objectives share identical gradients with respect to θ, while CFM offers the flexibility to choose the design choices of $u_t(x_t|x_1)$ and $p_t(x_t|x_1)$. A natural choice is to build the conditional probability paths as straight paths between the source and target distributions (Liu et al., 2023b; Lipman et al.,

2023), *i.e.*, $x_t = tx_0 + (1-t)x_1$. We can then use Equation 7 for training and solve the ODE from $t = 0$ to $t = 1$ to sample new data points.

C.2 Task Embedder

As shown in Fig. 11, introducing the task embedder helps adaptively cluster similar task instructions in the latent space while separating those from different tasks, guiding the model's generation process in the correct direction.

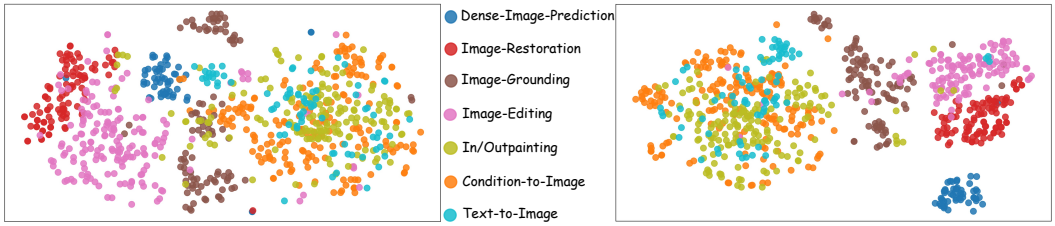

(a) t-SNE of embeddings before Task-Embedder (b) t-SNE of embeddings after Task-Embedder

Figure 11: t-SNE visualization of the global text embeddings. Each dot represents a user instruction.

C.3 Classifier-free Guidance for Multi-Modal Conditions

Classifier-free guidance (Ho & Salimans, 2022) is a technique that balances quality and diversity in images generated by a diffusion model. For our PixWizard, the network $e_\theta(z_t, c_I, c_T)$ has two conditionings: the input image c_I and text instruction c_T. Similar to InstructPix2Pix (Brooks et al., 2023) and InstructCV (Gan et al., 2024), we employ a tailored noise predictor that assigns different weights, w_I and w_T, to different conditionings, which can be adjusted to trade off how strongly the generated samples correspond with the input image and how strongly they correspond with the edit instruction. During training, we randomly set $c_I = \varnothing_I$ or $c_T = \varnothing_T$ for 5% of examples, and both conditions are $\varnothing$ for 5% of examples. The process is as follows:

$$\begin{aligned} \tilde{e_\theta}(z_t, c_I, c_T) = e_\theta(z_t, \varnothing, \varnothing) \\ + w_I \cdot (e_\theta(z_t, c_I, \varnothing) - e_\theta(z_t, \varnothing, \varnothing)) \\ + w_T \cdot (e_\theta(z_t, c_I, c_T) - e_\theta(z_t, c_I, \varnothing)) \end{aligned} \tag{8}$$

In Fig. 12, we illustrate the effects of the two parameters on the generated samples. As shown, changes in both W_I and W_T significantly influence the results. Specifically, in PixWizard, W_I strongly affects the color distribution of the generated images. An increase in W_I leads to more saturated and unrealistic colors. This can also negatively impact tasks such as depth estimation, where subtle depth variations may be represented as solid black regions. In contrast, the effects of W_T vary depending on the task. For example, in dense image prediction tasks, increasing W_T can degrade the quality of the estimation. However, for generative tasks, a higher W_T typically has little effect.

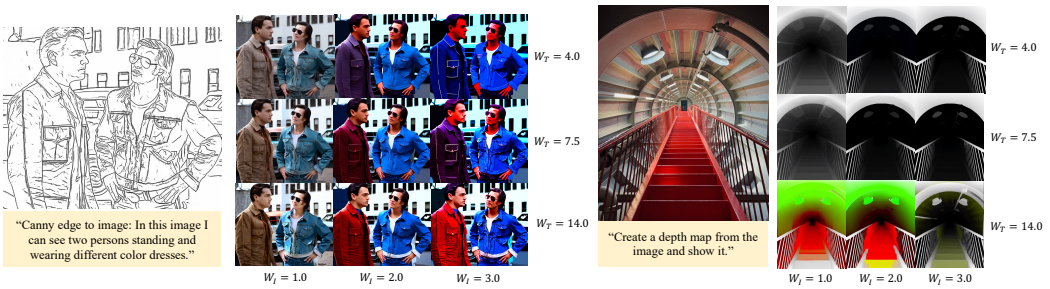

Figure 12: Impact of classifier-free guidance.

C.4 Any Resolution

PixWizard inherits the dynamic partitioning and padding scheme introduced by (Zhuo et al., 2024), allowing the model to handle images of any resolution and aspect ratio during both fine-tuning and inference.

The dynamic partitioning and padding scheme is introduced to optimize image token handling, avoiding fixed resolutions. Specifically, given constraints on the maximum number of patches and the maximum aspect ratio, the method defines a set of candidate patch partitions. For each input image size, it determines the optimal patch partition based on a matching ratio between the input size and the candidate partition, selecting the best fit. The input image is then resized accordingly using the chosen partition. This dynamic process leads to varying sequence lengths of patch tokens, so padding is applied to align the lengths across batches using a pad token. To prevent unwanted interactions between pad and regular tokens, attention masks are also introduced. This approach maximizes efficiency while preserving image integrity during embedding.

However, in practice, the required resolutions for different tasks can vary significantly. To support more flexible handling of arbitrary resolutions while preserving the original resolution as much as possible, we use $[512^2, 768^2, 1024^2]$ as resolution centers to generate candidate patch partitions. During training, we group data with similar resolutions into buckets, ensuring that sequence lengths within each batch are comparable, minimizing padding tokens, and improving training efficiency. During inference, by incorporating NTK-Aware Scaled RoPE (Peng & Quesnelle, 2023) and sandwich normalization, PixWizard demonstrates exceptional resolution extrapolation.

C.5 Inference Efficiency with Fewer Steps

Compared to diffusion-based methods (Gan et al., 2024; Hu et al., 2024; Wang et al., 2023c), our model demonstrates better inference efficiency under a low number of function evaluations (NFE) regime. By leveraging the linear interpolation schedule with flow matching objective, PixWizard can learn straighter trajectories, thus requiring fewer sampling steps to achieve decent performance. Drawing inspiration from the observation that flow-based models exhibit higher discretization error at the beginning of generation, we employ the shifted time schedule which allocates more steps near noise. By further integrating high-order ODE solvers with improved schedules, such as Heun and Midpoint, our model produces reasonable output using only 30-60 NFEs, compared to 100 NFEs used in diffusion-based counterparts.

D More Experimental Results

D.1 Implementation Details

Dense Image Prediction. For semantic segmentation, we assign labels by identifying the nearest neighbor RGB color value, and accuracy is evaluated using the Mean Intersection over Union (mIoU) metric. For monocular depth estimation, we average the output image across the three channels and apply the inverse of the linear transformation used during training to obtain depth estimates within the range of $[0, 10]$ meters. Accuracy is evaluated using the Root Mean Square Error (RMSE). For surface normal estimation, we recover the corresponding normal vectors from the output image and use the Mean Angle Error to assess accuracy.

Controllable Generation. We mainly evaluated PixWizard's ability based on two conditions: canny edge maps and depth maps. Following ControlNet++ (Li et al., 2024), we measured controllability using RMSE for depth maps and F1-Score for canny edges, comparing input conditions with features from the generated images. Image quality and text alignment were assessed using FID (Fréchet Inception Distance) and CLIP-Score. All experiments were conducted at a resolution of 512×512.

Image Inpainting. We used latent diffusion (Rombach et al., 2022b) to measure FID and LPIPS, focusing on samples where 40-50% of the image area was inpainted. For outpainting, we followed MaskGIT (Chang et al., 2022a) settings, extending the image by 50% and evaluating performance with FID and Inception Score (IS) on 512×512 crops from the Places dataset (2017a).

Text-to-image Generation. We evaluated PixWizard with two methods: visual examples and automatic metrics, including the Human Preference Score (HPS) v2 (Wu et al., 2023) and Zero-shot FID-30K on the MS-COCO dataset (Lin et al., 2014).

D.2 Image Restoration

Following previous works (Conde et al., 2024; Potlapalli et al., 2024; Ai et al., 2024), besides the results from the deraining and denoising benchmarks, we selected six additional image restoration tasks to further evaluate the robustness of PixWizard: Snow100K-L (Liu et al., 2018) for desnowing, Reside (outdoor) SOTS (Li et al., 2018) for dehazing, LOLv2 (Yang et al., 2021) for low-light enhancement, and GoPro (Nah et al., 2017) for deblurring. Additionally, to assess zero-shot capabilities on tasks not encountered during training, we use TOLED (Zhou et al., 2021) for under-display camera (UDC) image restoration and UIEB (Li et al., 2019a) for underwater (UW) image restoration. We evaluate performance using PSNR and SSIM as distortion metrics.

Table 5: Quantitative results on 6 restoration tasks with existing image restoration methods.

Methods	**Desnowing** Snow100K-L		**Dehazing** SOTS		**Low-light Enh.** LOLv2		**Deblurring** GoPro		**[Zero-shot](UDC)IR.** TOLED		**[Zero-shot](UW)IR.** UIEB	
	PSNR↑	SSIM↑	PSNR↑	SSIM↑	PSNR↑	SSIM↑	PSNR↑	SSIM↑	PSNR↑	SSIM↑	PSNR↑	SSIM↑
SwinIR (2021)	-	-	21.50	0.891	-	-	24.52	0.773	-	-	-	-
Restormer (2022)	30.98	0.914	24.09	0.927	20.77	**0.851**	27.22	0.829	27.74	0.841	**17.34**	**0.770**
NAFNet (2022a)	**31.42**	**0.920**	25.23	0.939	18.04	0.827	26.53	0.808	**27.90**	**0.848**	17.31	0.736
AirNet (2022)	30.14	0.907	21.04	0.884	19.69	0.821	24.35	0.781	26.76	0.799	17.09	0.761
PromptIR (2024)	30.91	0.913	**30.58**	**0.974**	21.23	0.860	27.02	0.798	-	-	-	-
DA-CLIP (2023)	28.31	0.862	30.16	0.936	**21.76**	0.762	24.65	0.703	-	-	-	-
InstructIR (2024)	-	-	26.90	0.952	-	-	**29.70**	**0.892**	-	-	-	-
PixWizard	29.66	0.883	28.14	0.937	20.29	0.807	24.68	0.774	27.22	0.826	16.99	0.752

Results. Table 5 presents a additional performance comparison with state-of-the-art (SOTA) task-specific and all-in-one restoration methods. As shown in the results, even though image restoration data constitutes only a small portion of the overall training data, our method still demonstrates competitive performance, even outperforming some task-specific methods. For example, it outperforms DA-CLIP in the desnowing task and exceeds NAFNet, Restormer, and AirNet in the dehazing task. Furthermore, when evaluated on tasks not included in the training phase, our method achieved performance comparable to that of specialized models, highlighting the generalizability of our approach.

D.3 Image Grounding

We evaluate referring segmentation tasks on the gRefCOCO (gRef) (Liu et al., 2023a), RefCOCO, and RefCOCO+ validation and test sets. To assess the performance gap between our approach and specialized models, we report results from several expert methods and primarily compare our approach with two unified models: Unified-IO (Lu et al., 2022b) and InstructDiffusion (Geng et al., 2024). Unified-IO directly produces the corresponding binary mask, while InstructDiffusion requires a post-processing network to extract masks from the output image. We use two comparison methods: (i) We convert the original image to the HSV color space to enhance the mask's hue, then apply a threshold for extraction. These results are reported as w/ HSV. (ii) We directly generate the corresponding binary mask for comparison. Following standard practices (Liu et al., 2023a), we use cumulative IoU (cIoU) to measure performance.

Results. Table 6 reports the results for referring segmentation. Our model demonstrates strong performance under two different mask extraction methods, outperforming InstructDiffusion across almost all evaluation datasets. In the various test sets of RefCOCO and RefCOCO+, our performance is comparable to Unified-IO, but on gRefCOCO, we significantly outperform Unified-IO (34.17 vs. 17.31). However, it is important to note that these unified methods still lag considerably behind those specifically designed for referring segmentation. Additionally, we observed that using a generative model for grounding tasks presents a significant challenge due to the model's limited perception and localization capabilities. This often results in failures to correctly locate objects when multiple targets are present, highlighting the need for improvements in instruction and understanding in future work.

Table 6: Quantitative results on referring segmentation in terms of cIoU.

Method	gRefCOCO	RefCOCO			RefCOCO+		
	val	val	test A	test B	val	test A	test B
CRIS 2022c	55.34	70.47	73.18	66.10	62.27	68.08	53.68
LAVT (2022)	57.64	72.73	75.82	68.79	56.86	62.29	48.14
ReLA (2023a)	62.42	73.21	75.24	68.72	56.10	62.26	47.89
Unified-IO (2022a)	17.31	46.42	**46.06**	**48.05**	**40.50**	**42.17**	40.15
InstructDiffusion w/ HSV (2024)	33.19	41.64	40.81	41.98	33.20	37.85	26.92
PixWizard w/ HSV	33.65	**47.28**	44.12	45.38	40.07	38.89	**40.76**
PixWizard	**34.17**	46.44	41.25	43.43	36.49	35.30	38.93

D.4 More Precise Editing

Based on the robust inpainting and grounding capability of PixWizard, we find that it allows user for more precise image editing tasks: *(i) Remove Anything.* It tackles the object removal problem (Criminisi et al., 2003; 2004; Elharrouss et al., 2020), enabling users to seamlessly remove specific objects. As shown in Fig. 13, PixWizard first generates a target mask based on user instructions, then fills the area with appropriate background details. *(ii) Replace Anything.* It lets users swap objects in an image, replacing them with specified objects while maintaining background consistency. *(iii) Add Anything.* This allows users to insert objects into an image. By adding a mask and providing a text prompt, PixWizard generates the desired content using its advanced inpainting ability.

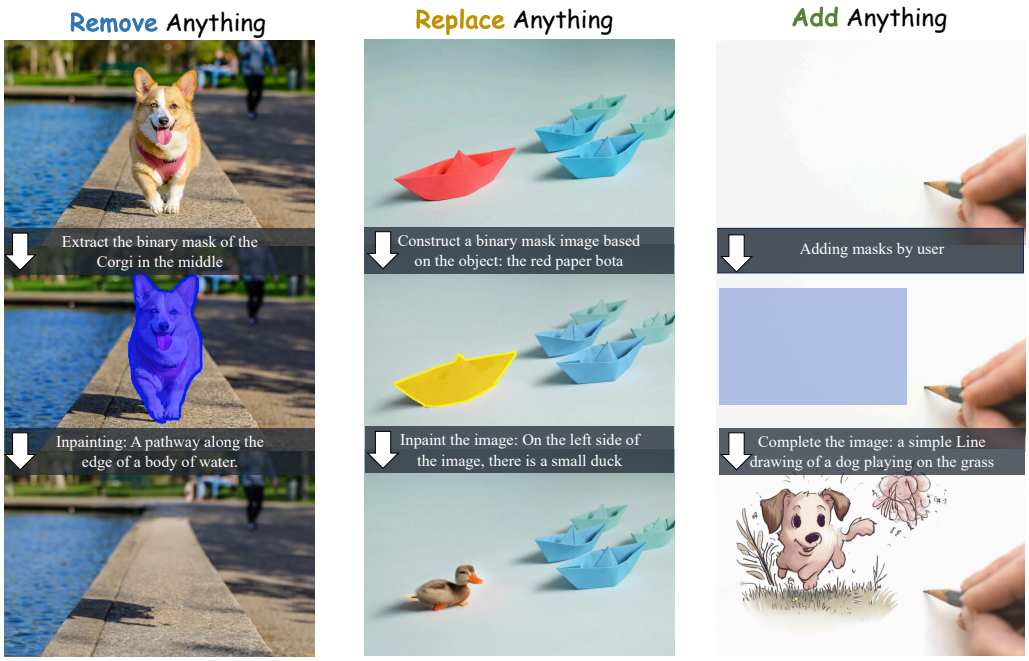

Figure 13: Visualization results of **Remove**, **Replace** and **Add** Anything.

D.5 Discussion on the Limitations of Image Editing Tasks

Image editing tasks can generally be divided into rigid and non-rigid edits. Rigid editing typically involves simpler modifications such as adding, removing, replacing, style transferring, or altering the texture of an object while maintaining the overall spatial structure of the image. On the other hand, non-rigid editing involves more complex transformations that require spatial manipulation, such as altering the pose of an object, swap the position or changing the viewpoint.

Despite the versatility of PixWizard in handling multiple types of rigid editing, we found that PixWizard currently exhibits limitations when dealing with non-rigid editing tasks, as several visualization

Make the boy close his eyes and smile.

Move the iPhone in the image to the right side of the image. Please help me close the book.

Figure 14: Bad cases of non-rigid editing.

examples shown in Figure. 14. When users attempt to provide more complex editing instructions, PixWizard often fails to execute them successfully, instead keeping the original image largely unchanged. This limitation arises primarily due to two reasons: the design of the structural-aware guidance module and the lack of diverse training data for non-rigid transformations. PixWizard's structural-aware guidance is implemented by concatenating the VAE latent representation with random noise along the channel dimension. We found that this method would limit generation directions to follow the structure of the input image, constraining its ability to perform non-rigid transformations that demand substantial structural alterations. However, it is worth noting that the "concat" method is efficient for other visual tasks such as image estimation, low-level tasks, and image grounding, which require maintaining similar structural characteristics. This is one of the reasons we initially adopted it. Furthermore, the datasets used to train PixWizard—such as UltraEdit (2024), MagicBrush (2024a), HQ-Edit (2024), Instruct P2P (2023), and SEED-X-Edit (2024)—focus predominantly on rigid editing tasks and lack non-rigid editing data pairs.

How to perform non-rigid editing in PixWizard is indeed one of the directions we aim to address. Here are some of our current thoughts: (1) Constructing non-rigid editing data pairs is important. This could involve utilizing state-of-the-art editing methods like Imagic (Kawar et al., 2023) and Forgedit (Zhang et al., 2023c), or advanced inpainting methods, complemented by GPT-assist and manual filtering to create high-quality non-rigid editing pairs. (2) Refining the structural-aware guidance. The primary objective is to move away from directly concatenating the VAE latent in the channel dimension. In future work, we aim to explore the integration of flow-based image inversion techniques and shift towards fusing targeted image features within the self-attention layers of the DiT block. Further experiments will be conducted to validate the effectiveness of this approach.

It is also worth mentioning that we found that the quality of most existing open-source image editing datasets is subpar. There are two main issues: first, the target images often contain artifacts, making them look unrealistic; second, there is a lack of alignment between the target images and the editing instructions. Through experiments, we discovered that simply using more open-source data does not necessarily lead to better performance. On the contrary, using a small amount of high-quality editing data results in better performance in both evaluation metrics and user experience with PixWizard. Therefore, it is both crucial and meaningful to explore methods for effectively cleaning open-source editing datasets. We are committed to addressing this issue in the future.

D.6 Generalization Ability to Unseen Tasks and Prompts

Zero-shot Examples. We have provided several zero-shot visual examples in Fig. 15. These include marking target objects using different symbols other than a box, such as a star, a point, or a circle. Additionally, we can change the color of detection boxes to colors that were not seen during training. Furthcerermore, we can simultaneously perform multiple tasks, such as joint deraining and watermark removal, deraining and super-resolution, or inpainting and outpainting, with masks of

any shape and mixed black-and-white colors. These examples highlight the generalizability of our approach. However, getting PixWizard to perform entirely new tasks that are completely unrelated to the training data, such as adding an object and then detecting it or contour detection, is challenging. This limitation points to the boundaries of PixWizard's generalization capabilities.

Few-shot Examples. Following Emu Edit's experimental setup (Sheynin et al., 2024), we further validated PixWizard's generalizability from a few-shot learning perspective. We prepared an object contour detection task as an illustration. We constructed 50 training samples for this task (all with red contours) and added them to our training dataset, then fine-tuned PixWizard. As shown in Fig. 15, PixWizard quickly acquired this capability. Additionally, we changed the contour color and found that PixWizard could still follow the instructions, implying that the model can effectively generalize to novel tasks.

Figure 15: Visualization results of zero-shot and few-shot.

D.7 Multi-Hot Gumbel-Softmax

In the implementation of the Multi-Hot Gumbel-Softmax (MHGS), the pseudocode is defined as follows:

```
def MHGS(logits, temp=1, dim=-1, sample_tokens=16):
    # Add Gumbel noise and scale by temperature
    gumbels = (logits + GumbelNoise(shape=logits.shape)) / temp

    # Apply Softmax to obtain soft outputs
    y_soft = Softmax(gumbels, dimension=dim)

    # Select top-k values for discrete output
    indices = Top-K(y_soft, k=sample_tokens, dimension=dim)

    # Create a hard multi-hot tensor from indices
    y_hard = MultiHotTensor(indices, shape=logits.shape)

    # Combine hard and soft outputs while preserving gradients
    ret = y_hard - StopGradient(y_soft) + y_soft

    return ret
```